# MULTIVARIABLE SENSOR NETWORK VIA WAVELENGTH ROUTER


KREANGSAK TAMEE



A THESIS SUBMITTED IN PARTIAL FULFILLMENT

OF THE REQUIREMENT FOR THE DEGREE OF

DOCTOR OF ENGINEERING IN ELECTRICAL ENGINEERING

FACULTY OF ENGINEERING

KING MONGKUT'S INSTITUTE OF TECHNOLOGY LADKRABANG

2011

KMITL-2011-EN-D-018-005

| | |
|---|---|
| **หัวข้อวิทยานิพนธ์** | เครือข่ายเซนเซอร์บนเราเตอร์แบบหลายความยาวคลื่น |
| **นักศึกษา** | นายเกรียงศักดิ์ เตมีย์ |
| **รหัสประจำตัว** | 46060207 |
| **ปริญญา** | วิศวกรรมศาสตรดุษฎีบัณฑิต |
| **สาขาวิชา** | วิศวกรรมไฟฟ้า |
| **พ.ศ.** | 2554 |
| **อาจารย์ที่ปรึกษาวิทยานิพนธ์** | รศ.ดร. สมศักดิ์ มิตะถา |

## บทคัดย่อ

วิทยานิพนธ์นี้นำเสนอการใช้อุปกรณ์ขนาดนาโนเมตรร่วมกับเครือข่ายสำหรับนำไปใช้งานด้านเซนเซอร์ ซึ่งสามารถเพิ่มประสิทธิภาพโดยเฉพาะอย่างยิ่งในเรื่องของความละเอียดระดับนาโนสเกล ประการแรกนำเสนอระบบใหม่ที่เป็นเซนเซอร์แบบมัลติฟังก์ชัน โดยการใช้ดาร์คและไบร์โซลิตอนในแมนเชลเตอร์อินเตอร์ฟีรอมิเตอร์ แนวคิดพื้นฐาน คือ คู่ของดาร์คและไบร์โซลิตอนภายในแมนเชลเตอร์อินเตอร์ฟีรอมิเตอร์จะเกิดขึ้นพร้อมกันได้ด้วยตัวควบคุมเฟส ดังสมุติฐาน “โซลิตอนทั้งสองรูปแบบเมื่อนำเข้าไปในแต่ละพอร์ตของแมนเชลเตอร์อินเตอร์ฟีรอ-มิเตอร์พร้อมกัน การเปลี่ยนแปลงเฟสสามารถเกิดขึ้นได้เมื่อแสงส่งผ่านไปยังตัวควบคุมเฟส และหน่วยวัดเซนเซอร์ ซึ่งในการปรับเพื่อดึงเฟสคืนด้วยตัวควบคุมเฟสจะมีความสัมพันธ์กัน สามารถนำไปทำเป็นเครื่องมือวัดได้” ประการที่สองนำเสนอเซนเซอร์และทรานสดิวเซอร์แบบใหม่ โดยใช้โพรงสั่นพ้องวงแหวนประเภท PANDA ประกอบไปด้วยตัวกรองแสงแอ็ด/ดร็อปที่มีวงแหวนข้างหนึ่งทำหน้าที่เป็นตัววัดและวงแหวนอีกข้างหนึ่งทำหน้าที่เป็นตัวอ้างอิง หลักการทำงาน คือ เมื่อมีผลกระทบจากภายนอกกระทำบนวงแหวนข้างที่เป็นตัววัดจะทำให้เกิดการเปลี่ยนแปลงค่าความยาวคลื่นเนื่องจากเส้นรอบวงของวงแหวนเปลี่ยนแปลง ผลจากการทดลองแสดงให้เห็นว่าความละเอียดในการวัดค่าการเปลี่ยนความยาวคลื่นอยู่ในระดับ 1 นาโนเมตร สุดท้ายแล้วระบบเซนเซอร์ดังกล่าวที่นำเสนอสามารถนำมาทำเป็นเซนเซอร์แบบกระจายผ่านทางเราเตอร์แบบหลายความยาวคลื่น ดังนั้นระบบเซนเซอร์นี้จึงเหมาะที่จะนำไปทำเป็นเครื่องมือวัดแบบมัลติเซนเซอร์ที่ค่าความละเอียดอยู่ในระดับนาโนเมตร

| | |
|---|---|
| **Thesis Title** | Multivariable Sensor Network via Wavelength Router |
| **Student** | Mr. Kreangsak Tamee |
| **Student ID.** | 46060207 |
| **Degree** | Doctor of Engineering |
| **Program** | Electrical Engineering |
| **Year** | 2011 |
| **Thesis Advisor** | Assoc. Prof. Dr. Somsak Mitatha |

## ABSTRACT

This thesis presents the use of nanoscale device to combine with the network base sensing application, which can be fulfilled the specific requirement of sensing applications, especially in the nanoscale resolution regime. Firstly, a new system of multi function sensors using dark and bright solitons in a Mach Zhender interferometer (MZI) is proposed. In this concept, the coincidence dark and bright soliton pair within the MZI can be arranged by using the phase controller. We assume that both solitons are input into the MZI ports simultaneously (coincidently). The randomly input dark and bright soliton states into the MZI ports can perform the change in phase after propagating through a phase shifter/sensing unit, in which the phase change recovery using the phase related measurement device can be provided. Secondly, we propose a new system of microring sensing transducer using a PANDA ring resonator type, in which the sensing unit is consisted of an optical add/drop filter and two nanoring resonators, where one ring is placed as a transducer (sensing unit), the other ring is set as a reference ring. In operation, the external force is assumed to exert on the sensing ring resonator. The obtained results have shown that the change in wavelength due to the change in sensing ring circumference is seen, in which the wavelength shift of 1 nm resolution is achieved. Finally, the distributed sensors presented via the multi wavelength router is generated by dark soliton pulses propagating within the ring resonator, which are allowed to form in the multi sensors (sensing transducers), which are formed by the sensing ring devices. The sensing system is suitable to perform the multi sensing measurements in the nano scale regime such as force, stress and temperature.

# ACKNOWLEDGEMENTS

I am greatly indebted to the people who have helped me make one of my lifetime dreams come true. This dream could have never become reality without the endless support and guidance of my advisor Assoc.Prof.Dr. Somsak Mitatha and Assoc.Prof.Dr. Ouen Pingern. I am grateful to Assoc.Prof.Dr. Preecha P. Yupapin for introducing me the research topics. I thank him for his unshaken belief in me and motivating me to reach to my goal. His tireless effort and inspiration has helped be immensely to be where I am today and to achieve what I have today.

Many thanks to every young members of the Advanced Research Center of Photonic Laboratory (ARCP) of the Department of Applied Physices, Faculty of Science, KMITL and every young members of the Hybrid Computing Research Laboratory (HCRL) of the Department of Computer Engineering, Faculty of Engineering, KMITL; whose support has created a friendly environment and the countless discussions we had kept me focused and always gave a different perspective to my work which helped me resolve many issues on the way.

It is my honor to have Assoc.Prof.Dr. Suvepon Sittichivapak, Asst.Prof.Dr. Suthichai Noppanakeepong and Asst.Prof.Dr. Phaophak Sirisuk in the committee.

The author is pleased to acknowledge the support from the Commission on Higher Education of Thailand, Computer Science and Information Technology, Faculty of Science, Naresuan University, Phitsanulok, Thailand

I am very grateful to my parents for their persistent encouragement to pursue higher studies. Finally, I would like to thank my beautiful wife and my beloved son for always keeping my spirits high, and encouraged me to go forward during difficult times.

**Kreangsak Tamee**

# CONTENTS

# CONTENTS (cont.)

# LIST OF FIGURES

# LIST OF FIGURES (cont.)

# LIST OF FIGURES (cont.)

**Figures** **Pages**

# CHAPTER 1

# INTRODUCTION

This chapter includes motivation of work, aim of work, structure of thesis and providing some fundamentals in subject of sensors. Optical sensors are presented in a relatively simple and straightforward way to give a tour through the subject by minimizing theoretical explanations and showing outstanding examples of what guided wave technology is able to offer for sensing.

## 1.1 Motivation

Optical Soliton has been recognized as a nonlinear solitary wave for years [1, 2]. Since then, it has been widely investigated in several subjects such as in physics, mathematics and communication, especially, in optical communication. Generally, the common property of a soliton known as self-phase modulation (SPM) and cross phase modulation(CPM) are the challenged behaviors. Furthermore, the non-dispersion behavior of the soliton is the key advantageous. This is capable the use in long-haul communication, where the long distance link without a repeater can be employed. Recently, several research works have shown that use of dark and bright soliton in various applications can be realized [3-8]. One has shown that the secured signals in the communication link can be retrieved by using a suitable add/drop filter that is connected into the transmission line. To date, there are many techniques that can be used to perform the nano-scale measurement resolutions and standards [9-11]. Recently, the use of a new form of a ring resonator called a PANDA ring resonator has shown the interesting aspect of applications [12, 13]. One of the interesting results is the use of a specific model of a ring resonator known as a PANDA ring resonator [14], which can be a good candidate for nanoscale sensing applications. For research and visitation there for in this thesis, we use of nanoscale device to combine with the network base sensing application, which can be fulfilled the specific requirement of sensing applications, especially in the nanoscale resolution regime and self-calibrations and more efficiency.

## 1.2 Aims of This Work

The aims and objectives of this work were:

**(a)** To investigates the simulation nonlinear micro and nano ring resonators and application, especially dark-bright signal amplification system, the concept of the dark-bright soliton conversion within add/drop optical filter system and soliton communication via a wavelength router

**(b)** To develop a new system of sensors using dark and bright solitons in a Mach Zhender interferometer (MZI). The advantage of the proposed system is that the multi functions in terms of phase shift sensor, orthogonal soliton (entangled photon) sensor, single photon sensor and self calibration measurement can be provided.

**(c)** To develop a new system of microring sensing transducer using a PANDA ring resonator type, in which the sensing unit is consisted of an optical add/drop filter and two nanoring resonators, where one ring is placed as a transducer (sensing unit), the other ring is set as a reference ring. The sensing and the reference signals are analyzed, simulated and compared.

**(d)** To show the multi wavelength router is generated by dark soliton pulses propagating within the resonator, which are allowed to form in the multi sensors (sensing transducers), which are formed by the sensing ring devices. The distributed sensing system is designed, which is available for network sensing applications.

## 1.3 Structure of the Thesis

The structure of the thesis is as follows.

**(a)** The current chapter gives an introduction to the subject of the thesis in term of optical sensors.

**(b)** Chapter 2 describe the theoretical background starts with general considerations of ring resonator and the used model for single coupler ring resonator filter (SCRR) and double coupler ring resonator filter (DCRR). Then, presents a very fascinating simulation of light pulses traveling within a ring resonator system that have revealed unexpected results for various applications, especially, in optical communication.

(c) Chapter 3 design a new system of sensors using dark and bright solitons in a Mach Zhender interferometer (MZI).

(d) Chapter 4 designs a new system of microring sensing transducer using a PANDA ring resonator type.

(e) Chapter 5 describe the use of multi dark solitons generated by using the multi light sources, which is also available for the distributed sensing system using the multi wavelength router.

(f) Finally, Chapter 6 presents a conclusion of the thesis and future work.

## 1.4 Optical Sensors

Optical sensors are essentially a means whereby light guided within an optical fiber or an optical waveguide can be modified in response to an external physical, chemical, biological or similar influence. Light from an optical source whose relevant optical properties, with respect to the sensing mechanism remains constant, is launched into an optical fiber and guided at a point at which measurement is to be made. At this point the light from the fiber is launched into a device which is specially designed in order to measure a specific measurand: a physical, chemical or biological quantity that needs to be sensed. The important advantage that fiber-optic sensors have over electronic sensors is the relative ease with which arrays for distributed sensing can be formed, and also the fact that there is a considerable potential for multiplexed fiber sensor systems in which the tremendous information carrying capacity of the optical fiber can be exploited.

The guided wave sensors that have been proposed to solve problems in industrial, automotive, avionic, military, geophysical, environmental and biomedical applications are countless. Sensors are presented in a relatively simple and straightforward way to give a tour through the subject by minimizing theoretical explanations and showing outstanding examples of what guided wave technology is able to offer for sensing. References to the extensive literature in this area are provided, where the interested reader can find more details. An increasing number of textbooks is also available [15-17].

### 1.4.1 Fiber and Integrated Optics: Fundamentals of Waveguiding

In accordance with the ray theory of light propagation, when light impinges at the interface between two transparent media, it is partially reflected and partially refracted. The Snell's law describes the refraction phenomena as (Fig. 1.1):

$$n_1 \sin\theta_1 = n_2 \sin\theta_2 \tag{1.1}$$

When $n_1 > n_2$, any ray impinging at the interface with an incident angle greater than $\theta_c$ is totally reflected inside the first medium.

$$\theta_c = \sin^{-1}\frac{n_2}{n_1} \tag{1.2}$$

An optical fiber consists of layered cylinders of glass or plastic, as shown in Fig.1.2. Inner and outer cylinders, namely 'core' and 'cladding', have refractive indices $n_1$ and $n_2$ , respectively. Any ray impinging at the core cladding interface with an incident angle greater than $\theta_c$ is undergoing multiple reflections within the core, in which it results trapped and propagates.

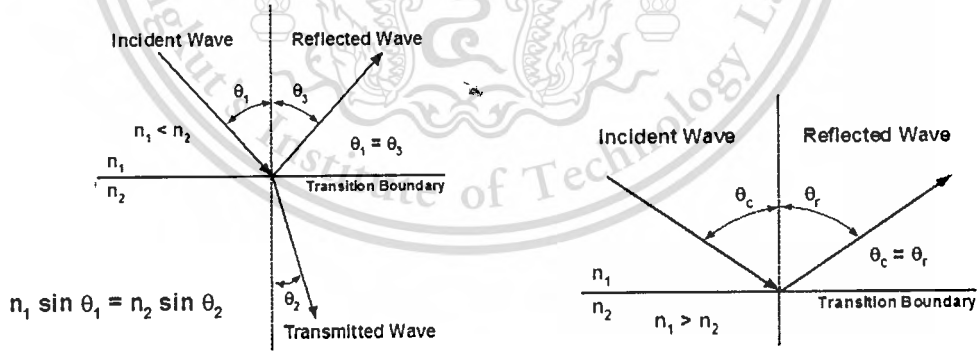


**Fig. 1.1** Reflection and refraction at the interface between two transparent media: the Snell law.

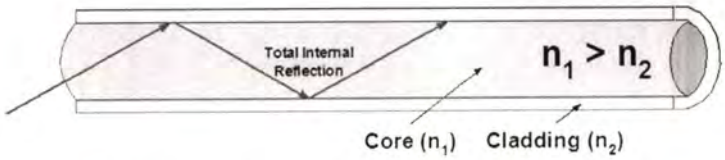


**Fig. 1.2** Ray propagation in the optical fiber.

### 1.4.2 Waveguide Sensors: Basic Working Principle

Although trapped within the dielectric medium of the optical waveguide, the radiation that propagates inside the waveguide can be perturbed by the external environment, and this perturbation can be used to draw useful information for sensing purposes. In fact, the interaction of the parameter of interest, which is the measurand, with the waveguide produces a modulation in the propagation constants of the guided light beam. That modulation represents the sensitive function of the measure of interest. As shown in Fig. 1.3, the basic elements constituting a guided wave sensor are: an optical source, an optical interface for source-to-waveguide light coupling, the waveguide itself where the measurand induced light modulation occurs, a photodetector and the electronics for amplification, signal processing and data display.

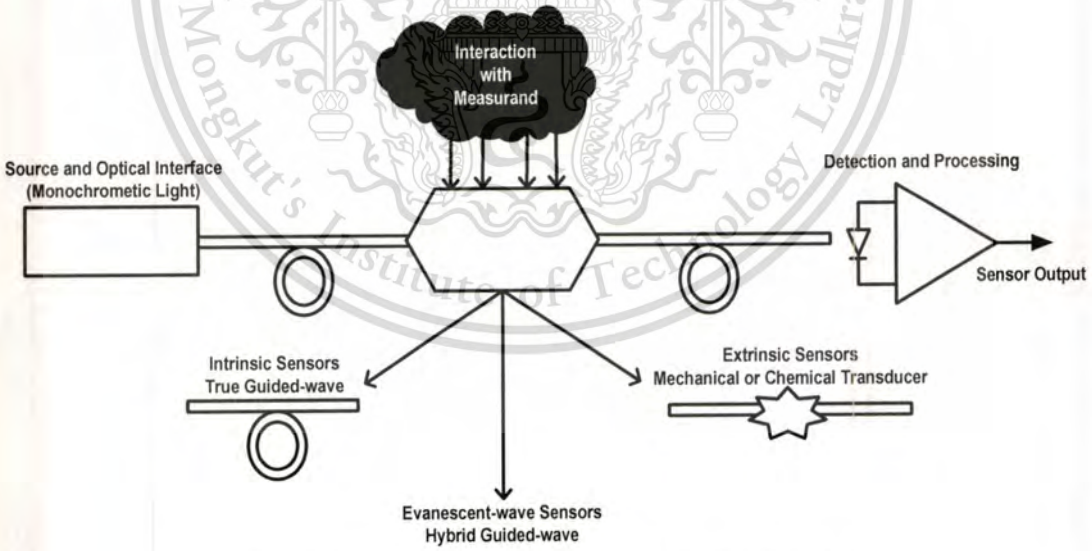


**Fig. 1.3** The waveguide sensor: general working principle.

In accordance to the optical parameter, which is modulated by the measurand, waveguide sensors can be divided into three basic categories:

- Phase-modulation,
- Wavelength-modulation,
- Intensity-modulation.

Waveguide sensors are further subdivided as intrinsic, extrinsic, or evanescent-wave sensors. In intrinsic fiber optic sensors, as shown in Fig. 1.3, the measurand interacts directly with the light in the fiber. Phase, polarization, and intensity may all be modulated within the fiber in an appropriate way. In the extrinsic fiber optic sensors, as shown in Fig. 1.3, the fiber may be used strictly as information carriers that lead up to a black box to impress information on a light beam that propagates to a remote receiver through a second or, in some cases, the same fiber. The black box may contains mirrors, a gas or liquid cell, a cantilevered arm, or dozens of other mechanisms that may generate, modulate, or transform a light beam. Evanescent-wave sensors are hybrid intrinsic/extrinsic sensors, since measurand-induced modulation occurs in the waveguide itself, in most cases because of the presence of a measurand-sensitive cladding section.

### 1.4.3 Interferometric Fiber Optic

A large and important subclass of intrinsic or all-fiber sensors are the interferometric fiber optic sensors, which have intrinsically highest sensitivity to environmental modulation, so that very high resolution measurements are feasible. Interferometric fiber optic sensors are the most promising among all the fiber optic sensors under study.

Interferometric fiber optic sensors evolve from traditional optical fiber interferometers. A range of optical fiber versions of classical interferometer configurations, such as the two-beam Mach Zehnder, Michelson, and Sagnac interferometers, and the multiple beam fiber Fabry-Perot and ring resonator configurations have been proposed. Fig. 1.4 shows these various implementations. In all the configurations, fiber directional couplers (DC) play a very important role. Fiber optic couplers, which have been well developed, can be used as beam splitters and reflectors to avoid diffraction losses associated with bulk optic elements and to offer greater flexibility and reliability.

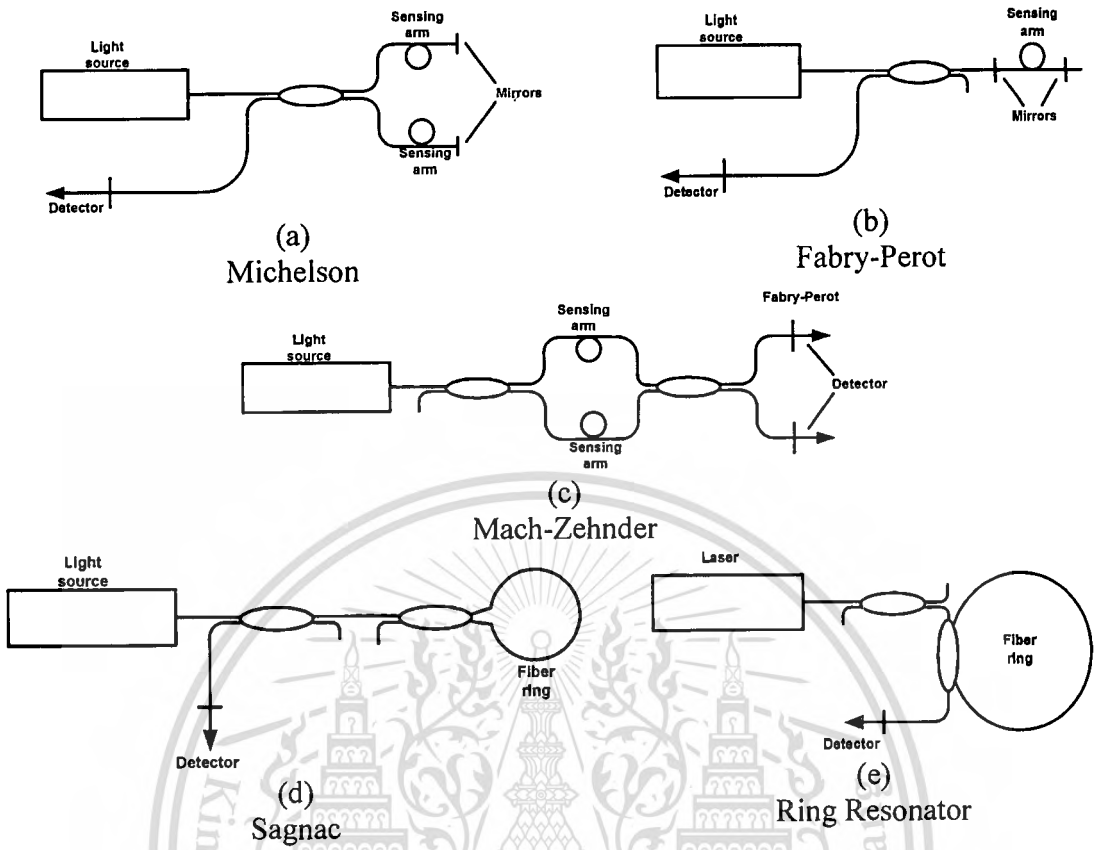


**Fig. 1.4** Interferometric fiber optic Michelson, Fabry-Perot, Mach-Zenhder, Sagnac, and ring resonator sensor configurations.

Generally speaking, fiber optic sensors based on two beam interference are less sensitive than fiber optic sensors based on multiple beam interference. On the other hand, although fiber optic sensors based on multiple beam interference have high sensitivity and may get rid of the "downlead sensitivity" problem, they must use highly coherent light source. Any phase noise, intensity noise, and frequency shift of light source will inevitably degrade the performance of the fiber optic sensors. Another disadvantage associated with fiber optic sensors based on Sagnac and multiple beam interferometers is that their unambiguous operating range is limited within a phase change of less than $\pi/2$. It should also be noted that in the fiber optic sensors based on Michelson, Sagnac, and Fabry-Perot interferometers there is a considerable amount of light feedback towards the light source,

which causes the light source unstable, especially when laser is used. A Farady isolator is most often needed to avoid the feedback.

In this thesis, we will be mostly concentrating on the two-beam Mach Zehnder Interferometers and the multiple beams Ring Resonator Interferometers. So we will describes the principle of operation of Mach Zehnder Interferometers and a micro-ring resonator for sensors application.

**Mach-Zehnder Interferometer for Sensor Applications**

The Mach-Zehnder configuration (Fig 1.5) is an intrinsic sensor based on the interference between a sensing and a reference wave. The two-beam interferometer uses a laser diode as the source of coherent light, which is coupled into a single mode fiber. The light is then split equally into two fibers by a 3-dB coupler. One arm of the Mach-Zehnder interferometer is the sensing arm while the other is the reference. The reference fiber is kept protected from the desired perturbation to be measured and light passes through this arm normally. The sensing fiber is used to monitor the perturbation. Two complementary outputs are available for signal processing.

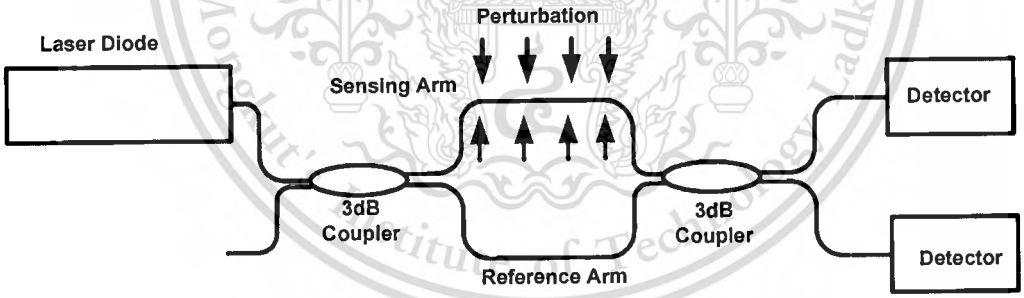


**Fig. 1.5** Mach-Zenhder Interferometer

The electric fields of the two light waves can be expressed as

$$E_r = E_0 e^{i\omega_0 t} \text{ and } E_s = E_0 e^{i(\omega_0 t + \Delta\phi)} \quad (1.3)$$

Where $E_r$ is the reference wave, $E_s$ is the sensing wave, and $\Delta\phi$ is the phase difference induced by the sensing fiber. At the photo detector, the intensity is given by [15]

$$I = \langle E_r^2 \rangle + \langle E_s^2 \rangle + 2\langle E_r E_s \rangle \tag{1.4}$$

Where $\langle\ \rangle$ represents the time integration performed by the photo detector. This equation reduces to

$$I = I_0(1 + \cos\Delta\phi) \tag{1.5}$$

Where $I_0 \alpha\ E_0^2$ and we have assumed in the ideal conditions of equal splitting ratios, no coherence or polarization effects, and no losses.

The information is contained in the phase difference between the two waves. The phase corresponding to a length of fiber L is

$$\phi = kn_{eff}L \tag{1.6}$$

Where $k = 2\pi/\lambda$ is the propogtion constant in air, $\lambda$ is the laser diode-emitting wavelength, and $n_{eff}$ is the fiber's effective refractive index. if the desired measured is X, then the change in $\phi$ may be represented by

$$\Delta\phi = kL\frac{dn_{eff}}{dX}\Delta X + kn_{eff}\frac{dL}{dX}\Delta X \tag{1.7}$$

If the coefficients $\frac{dn_{eff}}{dX}$ and $\frac{dL}{dX}$ for the sensing fiber are known, $\Delta X$can be found from the output signal, expressed by Eq. (1.5).

In this configuration, quantities such as strain, force, pressure, and temperature can be measured directly. Other quantities such as magnetic field, acoustic pressure, electric field, and current can be measured indirectly by attaching the sensing fiber to materials that respond to these parameters.

The output of the sensor, Eq. (1.8), is sinusoidal and is shown in Fig. 1.6. The signal goes through one period for every $2\pi$ shift in $\Delta\phi$. This period is referred to as one fringe.

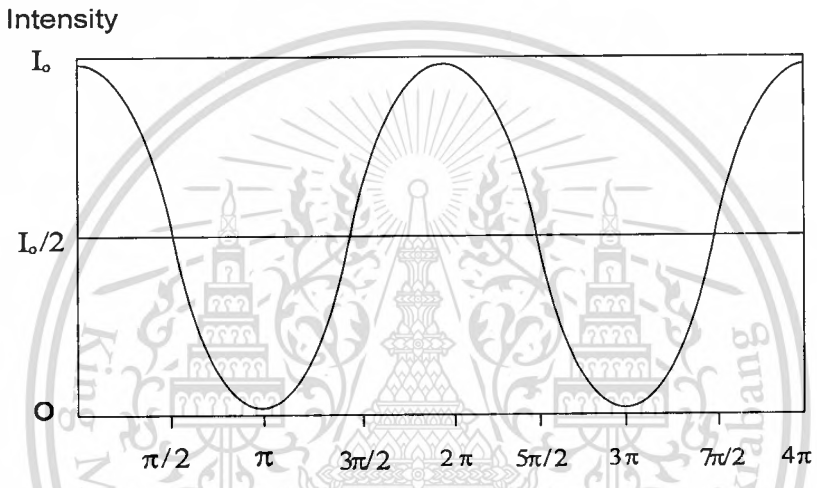


**Fig. 1.6** Mach-Zehnder Interferometer Output.

**Ring Resonator for Sensor Applications**

A ring resonator is simply a waveguide shaped into a ring structure as shown in Fig. 1.4(e). Consider, a waveguide coupled to a single micro-ring resonator. If there is an external force applied along the direction of the straight waveguide, the ring will distort, due to the effect of strain, $\varepsilon$, as shown in fig.1.7. The resonant wavelength of the ring resonator, $\lambda_m$, is given by

$$\lambda_m = \frac{nL}{m}, \tag{1.8}$$

Here, $m$ is integer, $n$ is the refractive index of the guiding material, and $L$ is the circumference of the ring resonator.

If the substrate upon which the polymer micro-resonator is fabricated is strained, the shape of the ring will be distorted which changes $L$ by $\Delta L$ and due to the strain-optic effect, changes the refractive index, $n$ by $\Delta n$.

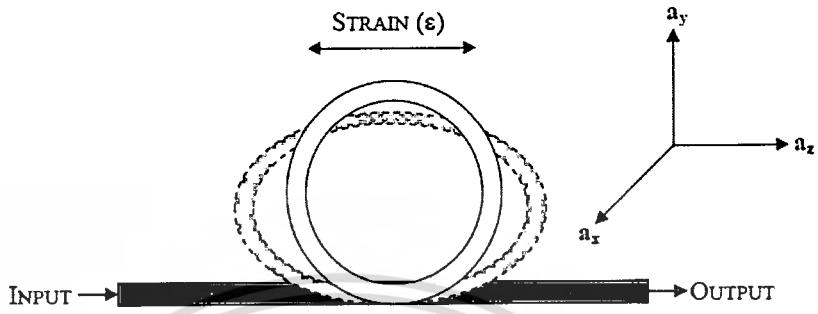


**Fig. 1.7** Schematic of a waveguide coupled micro-ring resonator and the effect of strain on the ring.

This shifts the resonant wavelength, $\lambda_m$, by $\Delta\lambda_m$ as

$$\frac{\Delta\lambda_m}{\lambda_m} = \frac{\Delta n}{n} + \frac{\Delta L}{L} \tag{1.9}$$

The first contribution for the shift in resonance is the change in $n$ which actually changes when the refractive index on the surface of the ring is modified by the interaction of analytes with sensing layer. Any mechanical effect leading to the change in the size of the ring structure could also modify the optical mode in the resonator and hence leading to a shift in the resonance wavelength.

# CHAPTER 2

# THEORETICAL BACKGROUND

Nonlinear fiber optics has continued to grow during the decade of 1990s, perhaps even more dramatically than anticipated. This growth is motivated by several recent advances in lightwave technology, the most important being the advent of high-capacity fiber-optic communication systems. A variety of nonlinear optical signal processing functions in micro ring resonator can be realized in many applications. For examples, the Kerr effect, four wave mixing (FWM) can be used to communication high microwave frequency (THz), the add/drop multiplexing can be used cancellation chaotic signal and the chaos of nonlinear system can be chaotic coding. In this chapter, we will describe the theoretical background of ring resonator starts with general considerations of ring resonator and the used model for single coupler ring resonator filter (SCRR) and double coupler ring resonator filter (DCRR). Then we will present a very fascinating simulation of light pulses traveling within a ring resonator system that have revealed unexpected results for various applications, especially, in optical communication. The design system consists of a nonlinear micro ring/nano ring resonator system incorporating an add/drop filter. Three different forms of input light pulses are Gaussian pulse, dark, and bright soliton, whereas the suitable simulation parameters are input power, pulse width, ring radii, and the material refractive indices.

## 2.1 Ring Resonators

A ring resonator is simply a waveguide shaped into a ring structure as shown in Fig. 2.1. When an input electric field, $E_i$, is coupled to the ring waveguide through an external bus waveguide, a positive feedback is induced and the field inside the ring resonator $E_r$, starts to build up. Coupling between the straight and the ring waveguide is achieved through the evanescent wave. Therefore, the gap and coupling length between them determine how much power is coupled from the straight waveguide to the ring waveguide and vise versa. In such configuration, only certain wavelengths will

be allowed to resonate inside the ring waveguide, thus frequency selectivity is obtained. A resonant mode will have a wavelength that satisfies.

$$m\lambda_m = nL, \quad \text{m = integer} \tag{2.1}$$

Here, $m$ is the longitudinal mode number, $\lambda_m$ is the resonant mode wavelength, $n$ is the refractive index of the guiding material, and $L$ is the circumference of the ring resonator.

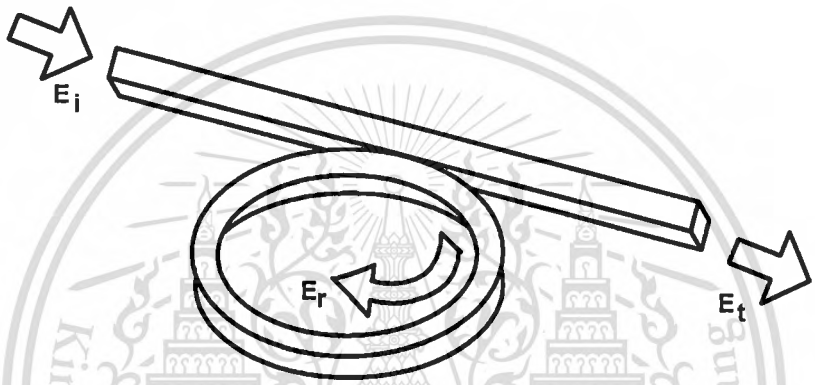


**Fig. 2.1** Schematic diagram for a ring resonator coupled to a single waveguide.

A ring resonator device is promising candidates for wavelength filtering, multiplexing/demultiplexing, conversion and network routing application. Two typical settings of ring resonator are shown in Fig. 2.2. A ring or a disk shaped dielectric cavity is placed between two parallel dielectric straight waveguides. In real life (3-D) devices, the straight waveguides can be positioned either in the same plane (Fig. 2.2(a): horizontal coupling scheme) or below (Fig. 2.2(b): vertical coupling scheme) the cavity plane. These two straight waveguides form four ports for the external connections, the two input ports named "In-port" And "Add-port", and the two output ports named "Through-port" and "Drop-port". To understand the functioning of the ring resonator, for the sake of simplicity, let's consider only unidirectional fields (clockwise propagating), where only the In-port is illuminated, while there is no incoming signal at the Add-port.

Conventionally, the functioning of ring resonator is described by the interaction of harmonic optical waves propagating along the straight waveguide and the cavity, and the interferometric

resonances of the waves inside the cavity. A single frequency optical wave is launched at the In port of the resonator. As this signal propagates along the upper straight waveguide, that connects the In-port and Through-port, part of it is evanescently coupled to the cavity. While propagating along the cavity, part of this signal is coupled to the lower straight waveguide and appears at the Drop-port. The remaining part of the signal propagates along the cavity, and interferes with the newly in-coupled signal in the upper interaction region. Depending upon the specific configuration, these two fields undergo constructive or destructive interference.

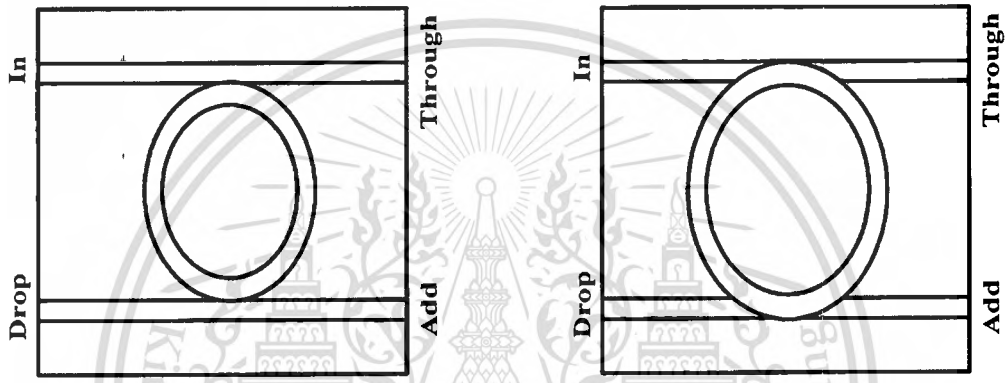


**Fig. 2.2** Scanning electron microscope pictures of horizontally coupled (a) and vertically coupled (b) real life ring resonator.

If the cavity field is out of phase with the newly entering field, then destructive interference takes place inside the cavity and as a result, there is only a small amount of power inside the cavity. Under so-called off resonance conditions, as shown in Fig. 2.3(a), most of the input power is directly transmitted to the Through-port, and there is comparably low power at the Drop-port.

On the other hand, if the field inside the cavity is in phase with the newly in-coupled signal, then due to constructive interference, energy builds up inside the cavity. This field gets coupled to the Drop-port waveguide. Under so-called resonance conditions, there is a signi_cant power observed at the Drop-port, while less power appears at the Through-port. This situation is shown in Fig. 2.3(b).

A typical spectral response of a ring resonator device is shown in Fig. 2.3(c). Resonance appears as dips in the Through-port power curve and peaks in the Drop-port power curve. In other words, the wavelength for which ring resonator is on resonance, will be "dropped" at the Drop port.

Also, for a symmetrical device, if a new signal that corresponds to a resonance wavelength is launched at the Add-port, it will get .added. to the off resonance signal launched at the input port, and appears at the throughput port. Therefore the arrangement shown in Fig. 2.2 can be used as an add/drop filter.

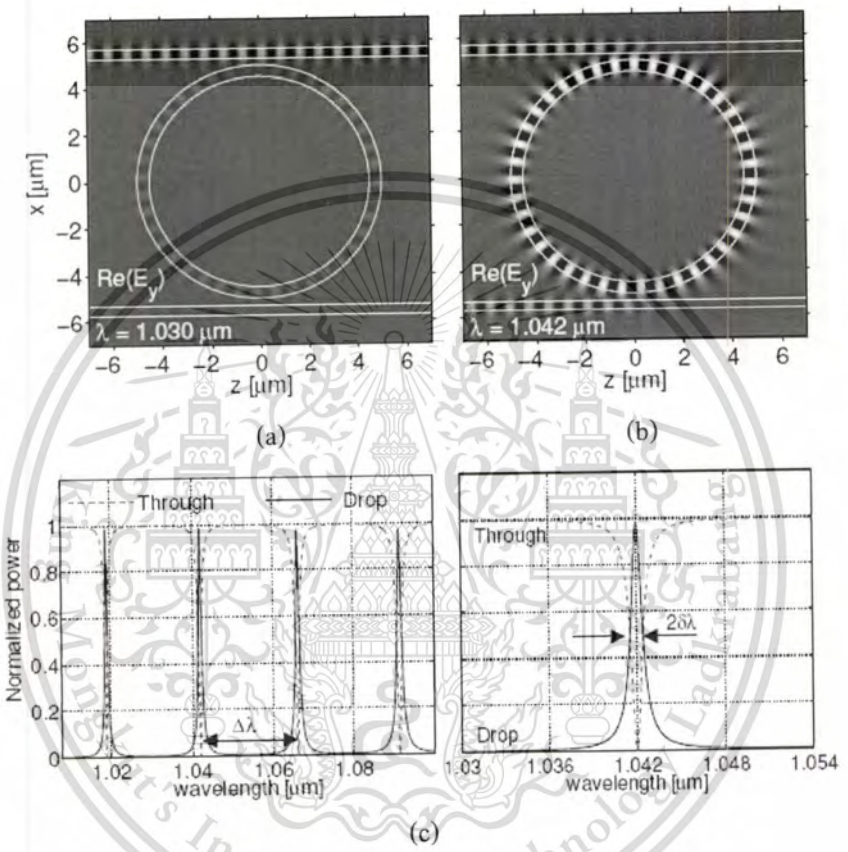


**Fig. 2.3** Simulated response off-resonance state (a) and resonance state (b) of a ring resonator. Also shown is the wavelength dependent response of the ring resonator (c).

## 2.2 The ring resonator – the used model

A single ring resonator is transferred into a box like filter shape using a single coupler or a double coupler configuration as shown in Figs 2.4 and 2.5. A calculation model is derived and all essential parameters describing the transmission characteristic are extracted in this section.

### 2.2.1 Single Coupler Ring Resonator Filter (SCRR)

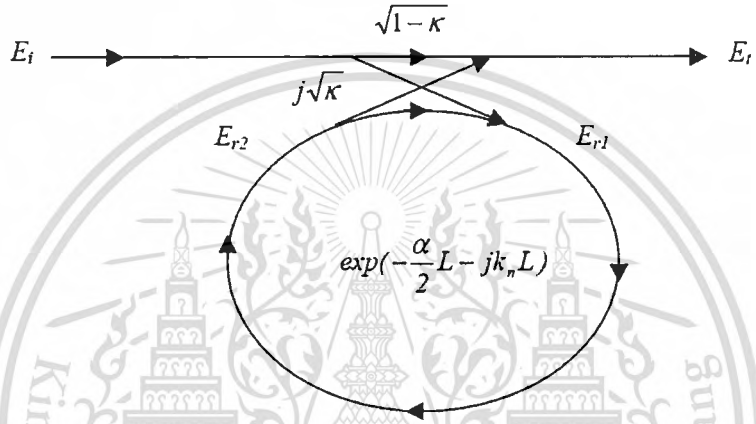


**Fig. 2.4** Schematic diagram for a ring resonator coupled to a single waveguide

The transfer function of this configuration is derived using Z-transform analysis. The circumference of the ring is $L$ ( $L = 2\pi R$, the radius is $R$ ), the coupling coefficient of the coupler is $\kappa$ . The Z-transform parameter is represented by $z^{-1} = \exp^{-jk_nL}$ where $k_n = \frac{2\pi}{\lambda} n_{eff}$ is the propagation constant and $n_{eff}$ is the effective index of the waveguide. The one round trip loss is $a = \exp^{-\alpha L/2}$, $\alpha$ is the intensity attenuation coefficient inside the waveguide [unit $length^{-1}$]. The transmitted or throughput field at the output of the straight waveguide, $E_t$ and inserted electric field, $E_i$ relations can be derived as followed:

$$E_t = (1-\gamma)^{1/2} \times \left[E_i \cdot \sqrt{1-\kappa} + j \cdot E_{r2}\sqrt{\kappa}\right]. \tag{2.2}$$

$$E_{r1} = (1-\gamma)^{1/2} \times \left[j \cdot E_i \cdot \sqrt{\kappa} + E_{r2} \cdot \sqrt{1-\kappa}\right]. \tag{2.3}$$

$$E_{r2} = E_{r1} \cdot a\, z^{-1}. \tag{2.4}$$

Using these equations, $E_t / E_i$ can be calculated:

$$\frac{E_t}{E_i} = (1-\gamma)^{1/2} \times \left[ \frac{\sqrt{1-\kappa} - (1-\gamma)^{1/2} \cdot a\, z^{-1}}{1-(1-\gamma)^{1/2} \cdot \sqrt{1-\kappa} \cdot a\, z^{-1}} \right]. \tag{2.5}$$

The transfer function in Eq. (2.5) indicates that a ring resonator is very similar to a Fabry-Perot cavity. In the particular case shown in Fig. 2.4, the corresponding Fabry-Perot cavity would have an input mirror with a field reflectivity and a fully reflecting output mirror. However, the field propagating inside the ring cavity is a traveling wave in contrast to the Fabry-Perot cavity which resonates a standing wave.

In the following, new parameter will be used for simplification:

$$\begin{aligned} D &= (1-\gamma)^{1/2} \\ x &= D \cdot \exp^{-\alpha L/2} \\ y &= \sqrt{1-\kappa} \\ \phi &= k_n \cdot L \end{aligned} \tag{2.6}$$

The intensity relation for the output port is given by:

$$T = \frac{I_t}{I_i}(\phi) = \left| \frac{E_t}{E_i} \right|^2 = D^2 \cdot \left[ 1 - \frac{(1-x^2)\cdot(1-y^2)}{(1-x\cdot y)^2 + 4\cdot x\cdot y\cdot sin^2\left(\frac{\phi}{2}\right)} \right]. \tag{2.7}$$

### 2.2.2 Double Coupler Ring Resonator Filter (DCRR)

Consider the architectures of double coupler ring resonator which sometime called add/drop filters as illustrated in Fig. 2.5, which are constructed by 2×2 optical couplers.

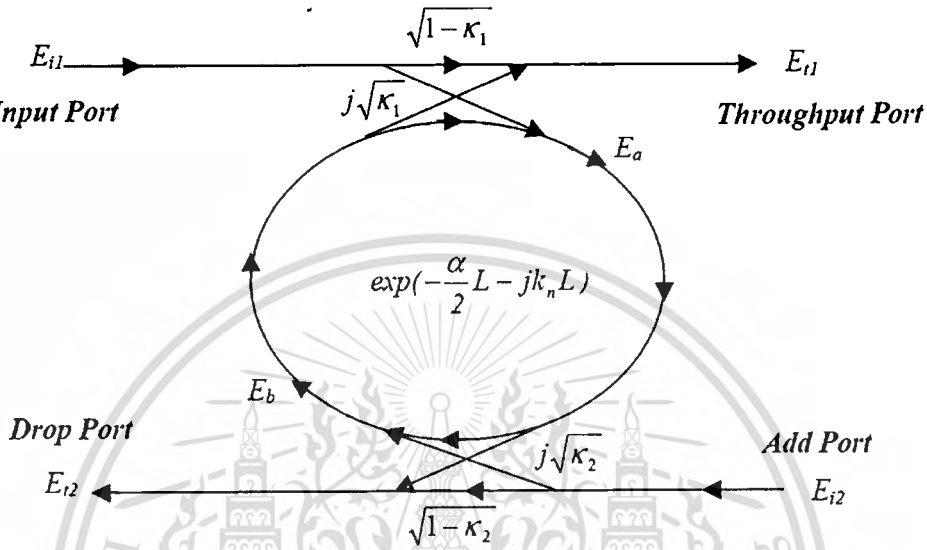


**Fig. 2.5** The single ring resonator with two adjacent waveguides

For simplification, the calculation of the intensity relation does not take into account coupling losses ($D^2 = 1$).

$$E_a = E_{i1} j\sqrt{\kappa_1} + E_b \sqrt{1-\kappa_1}\, e^{-\frac{\alpha L}{2\,2} - jkn\frac{L}{2}} \tag{2.8}$$

$$E_b = E_a \sqrt{1-\kappa_2}\, e^{-\frac{\alpha L}{2\,2} - jkn\frac{L}{2}} \tag{2.9}$$

$$E_a = \frac{E_{i1} j\sqrt{\kappa_1}}{1-\sqrt{1-\kappa_1}\sqrt{1-\kappa_2}\, e^{-\frac{\alpha}{2}L - jknL}} \tag{2.10}$$

$$E_b = \frac{E_{i1} j\sqrt{\kappa_1}}{1-\sqrt{1-\kappa_1}\sqrt{1-\kappa_2}\, e^{-\frac{\alpha}{2}L - jknL}} \cdot \sqrt{1-\kappa_2}\, e^{-\frac{\alpha L}{2\,2} - jkn\frac{L}{2}} \tag{2.11}$$

$$E_{t1} = E_b\, j\sqrt{\kappa_1}\; e^{-\frac{\alpha L}{2\,2} - jkn\frac{L}{2}} + E_{i1}\sqrt{1-\kappa_1} \tag{2.12}$$

$$E_{t2} = E_a\, j\sqrt{\kappa_2}\; e^{-\frac{\alpha L}{2\,2} - jkn\frac{L}{2}} \qquad at\;\; E_{t2} = 0 \tag{2.13}$$

Where $E_{i1}$ is the input field, $E_{t1}$ is the throughput field, $E_{t2}$ is the dropped field, $E_{t1}$, $E_a$ and $E_b$ are the fields in the ring, $\kappa_1$ is thefield coupling coefficient between the input bus and the ring, $\kappa_2$ is the field coupling coefficient between the ring and the input bus, $L$ is the circumference of the ring,

By using the upper equations, the transfer function for throughput port and drop port in Fig. 2.5 can thus be expressed as

**Throughput port:**

$$\frac{E_{t1}}{E_{i1}} = \frac{-\kappa_1\sqrt{1-\kappa_2}\; e^{-\frac{\alpha}{2}L - jknL} + \sqrt{1-\kappa_1} - (1-\kappa_1)\sqrt{1-\kappa_2}\; e^{-\frac{\alpha}{2}L - jknL}}{1 - \sqrt{1-\kappa_1}\sqrt{1-\kappa_2}\; e^{-\frac{\alpha}{2}L - jknL}} \tag{2.14}$$

$$\frac{E_{t1}}{E_{i1}} = \frac{-\sqrt{1-\kappa_2}\; e^{-\frac{\alpha}{2}L - jknL} + \sqrt{1-\kappa_1}}{1 - \sqrt{1-\kappa_1}\sqrt{1-\kappa_2}\; e^{-\frac{\alpha}{2}L - jknL}} \tag{2.15}$$

**Drop port:**

$$\frac{E_{t2}}{E_{i1}} = \frac{-\sqrt{\kappa_1\kappa_2}\; e^{-\frac{\alpha L}{2\,2} - jkn\frac{L}{2}}}{1 - \sqrt{1-\kappa_1}\sqrt{1-\kappa_2}\; e^{-\frac{\alpha}{2}L - jknL}} \tag{2.16}$$

The intensity relations for the throughput and drop port can be obtained by normalizing the transfer functions in Eqs. (2.17) and (2.18) which are given by

$$\frac{I_{t1}}{I_{i1}} = \left|\frac{E_{t1}}{E_{i1}}\right|^2 = \frac{1-\kappa_1 - 2\sqrt{1-\kappa_1}\sqrt{1-\kappa_2}\; e^{-\frac{\alpha}{2}L}\cos(knL) + (1-\kappa_2)e^{-\alpha L}}{1 + (1-\kappa_1)(1-\kappa_2)e^{-\alpha L} - 2\sqrt{1-\kappa_1}\sqrt{1-\kappa_2}\; e^{-\frac{\alpha}{2}L}\cos(knL)} \tag{2.17}$$

$$\frac{I_{t2}}{I_{i1}} = \left|\frac{E_{t2}}{E_{i1}}\right|^2 = \frac{\kappa_1 \kappa_2 e^{-\frac{\alpha}{2}L}}{1+(1-\kappa_1)(1-\kappa_2)e^{-\alpha L} - 2\sqrt{1-\kappa_1}\sqrt{1-\kappa_2}\, e^{-\frac{\alpha}{2}L}\cos(knL)} \tag{2.18}$$

## 2.3 Pulse Propagating within Micro Ring Resonator

Three different forms of input light pulses are Gaussian pulse, dark, and bright soliton.

### 2.3.1 Gaussian Pulse

Light from a monochromatic light source is launched into a ring resonator with constant light field amplitude ($E_0$) and random phase modulation as shown in Fig 2.6. The combination of terms in attenuation ($\alpha$) and phase($f_0$) constants results in a temporal coherence degradation. Hence, the time dependent input light field ($E_{in}$), without pumping term [18], can be expressed as

$$E_{in}(t) = E_0 e^{(-\alpha L + j\phi_0(t))} \tag{2.19}$$

where $L$ is a propagation distance(waveguide length).

We assume that the nonlinearity of the optical ring resonator is of the Kerr-type, i.e., the refractive index is given by

$$n = n_0 + n_2 I = n_0 + (\frac{n_2}{A_{eff}})P, \tag{2.20}$$

where $n_0$ and $n_2$ are the linear and nonlinear refractive indexes, respectively. $I$ and $P$ are the optical intensity and optical power, respectively. The effective mode core area of the device is given by $A_{eff}$. For the micro ring and nano ring resonators, the effective mode core areas range from 0.10 to 0.50 $\mu m^2$ [19, 20]

When a Gaussian pulse is input and propagated within a fiber ring resonator, the resonant output is formed, thus, the normalized output of the light field is the ratio between the output and input fields ( $E_{out}(t)$ and $E_{in}(t)$) in each roundtrip [21], which can be expressed as

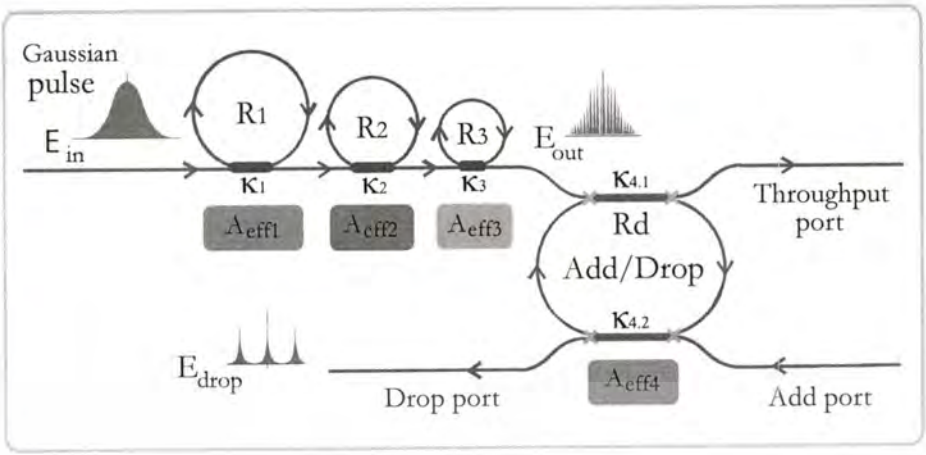


**Fig 2.6**. A schematic of a Gaussian soliton generation system, where $R_s$: ring radii, $K_s$: coupling coefficients, $R_d$: an add/drop ring radius, $A_{effs}$: Effective areas.

$$\left|\frac{E_{out}(t)}{E_{in}(t)}\right|^2 = (1-\gamma)\left[1 - \frac{(1-(1-\gamma)x^2)\kappa}{(1-x\sqrt{1-\gamma}\sqrt{1-\kappa})^2 + 4x\sqrt{1-\gamma}\sqrt{1-\kappa}\sin^2(\frac{\phi}{2})}\right] \quad (2.21)$$

Eq. (2.21) indicates that a ring resonator in this particular case is very similar to a Fabry-Perot cavity, which has an input and output mirror with a field reflectivity, (1- $\kappa$ ), and a full reflecting mirror. k is the coupling coefficient, and $x = \exp(-\alpha L/2)$ represents a roundtrip loss coefficient, $\phi_0 = kLn_0$ and $\phi_{NL} = kL(\frac{n_2}{A_{eff}})P$ are the linear and nonlinear phase shifts, $k = 2\pi/\lambda$ is the wave propagation number in a vacuum. Where L and $\alpha$ are a waveguide length and linear absorption coefficient, respectively. In this work, the iterative method is introduced to obtain the results as shown in Eq. (2.20), similarly, when the output field is connected and input into the other ring resonators.

The input optical field as shown in Eq. (2.19), i.e., a Gaussian pulse, is input into a nonlinear microring resonator. By using the appropriate parameters, the chaotic signal is obtained by using Eq. (2.21). To retrieve the signals from the chaotic noise, we propose to use the add/drop device with the appropriate parameters. The optical outputs of a ring resonator add/drop filter can be given by the Eqs. (2.22) and (2.23).

$$\left|\frac{E_t}{E_{in}}\right|^2 = \frac{(1-\kappa_1)-2\sqrt{1-\kappa_1}\cdot\sqrt{1-\kappa_2}e^{-\frac{\alpha}{2}L}\cos(k_nL)+(1-\kappa_2)e^{-\alpha L}}{1+(1-\kappa_1)(1-\kappa_2)e^{-\alpha L}-2\sqrt{1-\kappa_1}\cdot\sqrt{1-\kappa_2}e^{-\frac{\alpha}{2}L}\cos(k_nL)} \quad (2.22)$$

and

$$\left|\frac{E_d}{E_{in}}\right|^2 = \frac{\kappa_1\kappa_2 e^{-\frac{\alpha}{2}L}}{1+(1-\kappa_1)(1-\kappa_2)e^{-\alpha L}-2\sqrt{1-\kappa_1}\cdot\sqrt{1-\kappa_2}e^{-\frac{\alpha}{2}L}\cos(k_nL)} \quad (2.23)$$

where $E_t$ and $E_d$ represents the optical fields of the throughput and drop ports, respectively. The transmitted output can be controlled and obtained by choosing the suitable coupling ratio of the ring resonator, which is well derived and described by [21]. Where $\beta = kn_{eff}$ represents the propagation constant, $n_{eff}$ is the effective refractive index of the waveguide, and the circumference of the ring is $L = 2\pi R$, here $R$ is the radius of the ring. In the following, new parameters will be used for simplification, where $\phi = \beta L$ is the phase constant. The chaotic noise cancellation can be managed by using the specific parameters of the add/drop device, which the required signals at the specific wavelength band can be filtered and retrieved. $\kappa_1$and $\kappa_2$ are coupling coefficient of add/drop filters, $k_n = 2\pi/\lambda$ is the wave propagation number for in a vacuum, and the waveguide (ring resonator) loss is $\alpha$ = 0.5 dBmm$^{-1}$. The fractional coupler intensity loss is $\gamma$ = 0.1. In the case of an add/drop device, the nonlinear refractive index is neglected.

From Fig. 2.6, in principle, light pulse is sliced to be the discrete signal and amplified within the first ring, where more signal amplification can be obtained by using the smaller ring device (second and third ring). Finally, the required signals can be obtained via a drop port of the add/drop filter. In operation, an optical field in the form of Gaussian pulse from a laser source at the specified center wavelength is input into the system.

From Fig. 2.7, the Gaussian pulse with center wavelength ($\lambda_0$) at 1.30 μm, pulse width of 20 ns, peak power at 2 W is input into the system as shown in Fig. 2.7(a). The large bandwidth signals can be seen within the first, second microring and third nanoring device, and shown in Fig. 2.7(b), 2.7(c) and 2.7(d)., respectively. The suitable ring parameters are used, for instance, ring radii $R_1$ = 15.0 μm, $R_2$ = 10.0 μm, $R_3$ = 5.0 μm, and $R_d$ = 155.0 μm. Result of the spatial pulses with center wavelength at 1.30 μm, Fig. 2.7(e), the large bandwidth signals, Fig. 2.7(f), the filtering and

amplifying signals from the drop port. The smallest free spectrum range (FSR) and spectral width ($\Delta\lambda$) of 535 and 20 pm are generated respectively. The maximum output power is 40 W which is available for high capacity and long distance communication link.

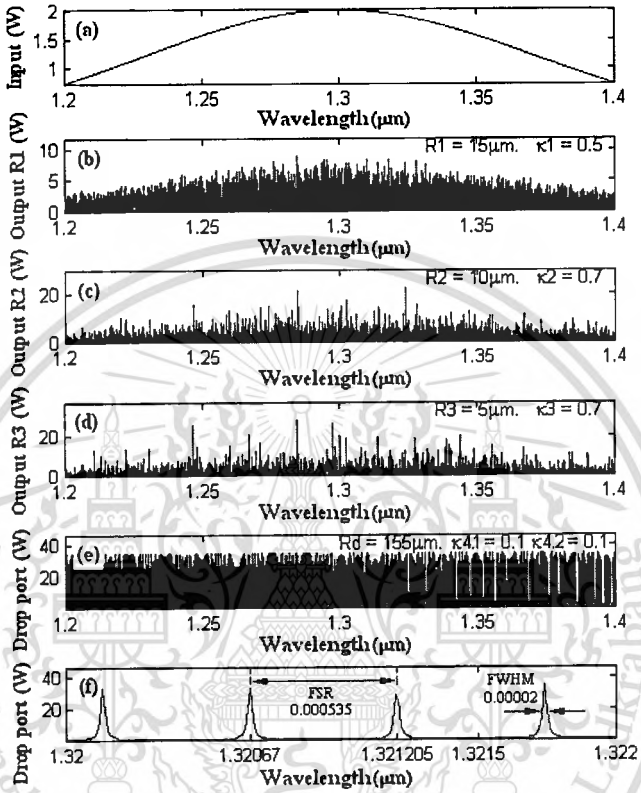


**Fig.2.7.** Result of the spatial pulses with center wavelength at 1.3 μm

By using the propose design, the extended light source wavelengths can be used for DWDM, which can be used with the existed public networks, the higher channel capacity can also be obtained by using FSR modification and more available wavelength bands, for instance, from near to far infrared wavelength bands. The smallest FSR obtained is about 500 pm as shown in Fig.2.7. Furthermore, the non-dispersive wavelength (1.30 μm) can be extended and used to increase the communication capacity, moreover, the Gaussian pulse output power can be amplified, which can provide the power budget for long distance link, which can be used with the existed public network installation, the pumping is not required in such a system [22].

### 2.3.2 Dark and Bright Solitons

A Gaussian pulse has been recognized as a laser pulse which can be used in both theoretical and experimental investigation for many subjects. However, in some ways, the limit of laser power can cause a problem, especially, when the high output power or long distance link is required. Optical soliton becomes a powerful tool that can overcome such a problem, i.e., a high power laser source. Furthermore, the non-dispersion of soliton in medium is the other advantage. Optical solitons can naturally be divided into classes of dark and bright solitons, whereas a dark soliton exhibits an interesting and remarkable behavior, when it is transmitted into an optical transmission system. It has the advantage of the signal detection difficulty, when the ambiguity of signal detection becomes a problem for the un-wanted users. In principle, the soliton generations and their behaviors in media are well analyzed and described by Agarwal [23]. Many earlier theoretical and experimental works on soliton applications can be found in the soliton application book by Hasegawa [24]. However, to make such a tool more useful, the problems of soliton-soliton interactions [25], collision [26], rectification [1], and dispersion management [2] must be solved and addressed. Therefore, in this work, we are looking for a powerful laser source with a broad spectrum that can be used in many applications.

Bright and dark soliton pulses are introduced into the multi-stage nano ring resonators as shown in Fig. 2.8, the input optical field ($E_{in}$) of the bright and dark soliton pulses input are given by an Eqs. (2.24) and (2.25) [23], respectively.

$$E_{in}(t) = A\sec h\left[\frac{T}{T_0}\right]\exp\left[\left(\frac{z}{2L_D}\right) - i\omega_0 t\right] \tag{2.24}$$

and

$$E_{in}(t) = A\tanh\left[\frac{T}{T_0}\right]\exp\left[\left(\frac{z}{2L_D}\right) - i\omega_0 t\right] \tag{2.25}$$

where $A$ and $z$ are the optical field amplitude and propagation distance, respectively. $T$ is a soliton pulse propagation time in a frame moving at the group velocity, $T=t-\beta_1 z$, where $\beta_1$ and $\beta_2$ are the coefficients of the linear and second-order terms of Taylor expansion of the propagation constant. $L_D=T_0^2/|\beta_2|$ is the dispersion length of the soliton pulse. $T_0$ in equation is a soliton pulse propagation

time at initial input (or soliton pulse width), where $t$ is the soliton phase shift time, and the frequency shift of the soliton is $\omega_0$. This solution describes a pulse that keeps its temporal width invariance as it propagates, and thus is called a temporal soliton. When a soliton peak intensity $\left(\left|\beta_2/\Gamma T_0^2\right|\right)$ is given, then $T_0$ is known. For the soliton pulse in the micro ring device, a balance should be achieved between the dispersion length ($L_D$) and the nonlinear length ($L_{NL}=1/\Gamma\phi_{NL}$), where $\Gamma=n_2k_0$, is the length scale over which dispersive or nonlinear effects makes the beam become wider or narrower. For a soliton pulse, there is a balance between dispersion and nonlinear lengths, hence $L_D = L_{NL}$. Similarly, the output soliton of the system can be calculated by using Gaussian equations as given in the previous case.

#### 2.3.2.1 Soliton Amplification

The dark and bright signal amplification system is shown in Fig. 2.8. Firstly, when the bright soliton system is operated, the large bandwidth within the micro ring device can be generated by using a bright soliton pulse input into the nonlinear micro ring resonator as shown in Fig. 2.9. Similarly, the input dark soliton pulse is chopped (sliced) into a smaller signal spreading over the spectrum as shown in Fig. 2.10, which is shown that the large bandwidth signal is generated within the first ring device. A soliton pulse with 50 ns pulse width, and maximum power at 0.65 W is input into the system. The results are obtained when a bright soliton pulse is input into the ring resonator system, whereas the parameters used are $R_1$= 10 μm, $A_{eff1}$ = 0.50 $\mu m^2$, $R_2$= 7 μm, $A_{eff2}$ = 0.25 $\mu m^2$, $R_3$= 5 μm, $A_{eff3}$ = 0.10 $\mu m^2$ and $\kappa_1$ = 0.2 and $\kappa_2$ = $\kappa_3$ = 0.05. The continuous spectra output which is 25 times larger than the input, it is obtained and seen in Fig. 2.9(c), secondly, a dark soliton pulse is input into a microring resonator system within NRR, where the parameters used are $R_1$= 10 μm, $A_{eff1}$ = 0.50 $\mu m^2$, $R_2$= 7 μm, $A_{eff2}$ = 0.25 $\mu m^2$, $R_3$= 5 μm, $A_{eff3}$ = 0.10 $\mu m^2$ and $\kappa_1$ = 0.2 and $\kappa_2$ = $\kappa_3$ = 0.05, then a dark soliton pulse is sliced into the smaller signals as shown in Fig. 2.10(a). Figs 2.10 (b) and 2.10 (c) are the output signals of the filtering signals within the rings $R_2$ and $R_3$. Results obtained when a dark soliton pulse is input into a micro and nanoring resonator system as shown in Fig. 2.10 (b). The continuous spectra output with 25 times larger than the input is obtained and seen in Fig. 2.10 (c). The coupling coefficients are given as shown in the figures.

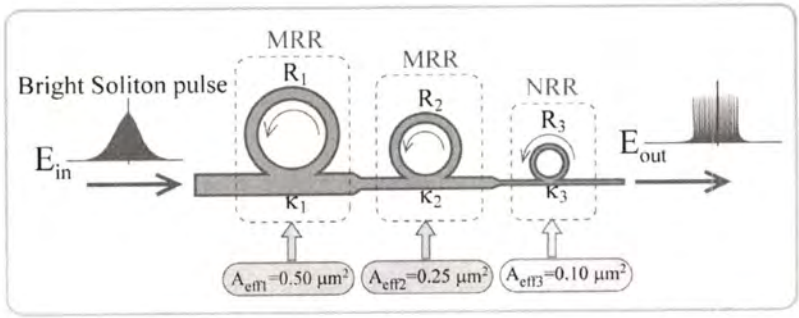


(a) Amplified bright soliton within NRR.

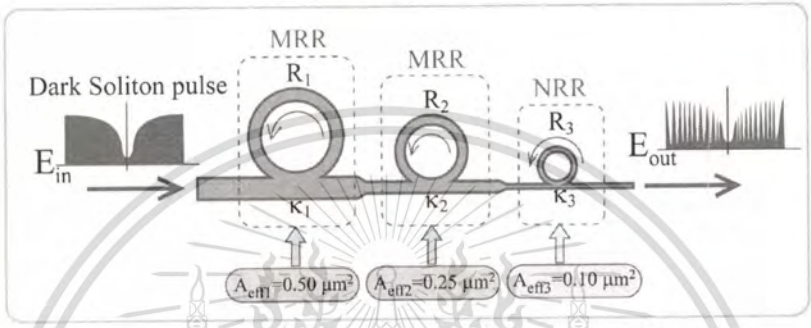


(b) Amplified dark soliton within NRR.

**Fig. 2.8** A schematic of the amplified dark-bright soliton conversion system, where $R_s$: ring radii and $K_s$: coupling coefficients, where MRR: Micro ring resonator, NRR:Nano-ring resonator.

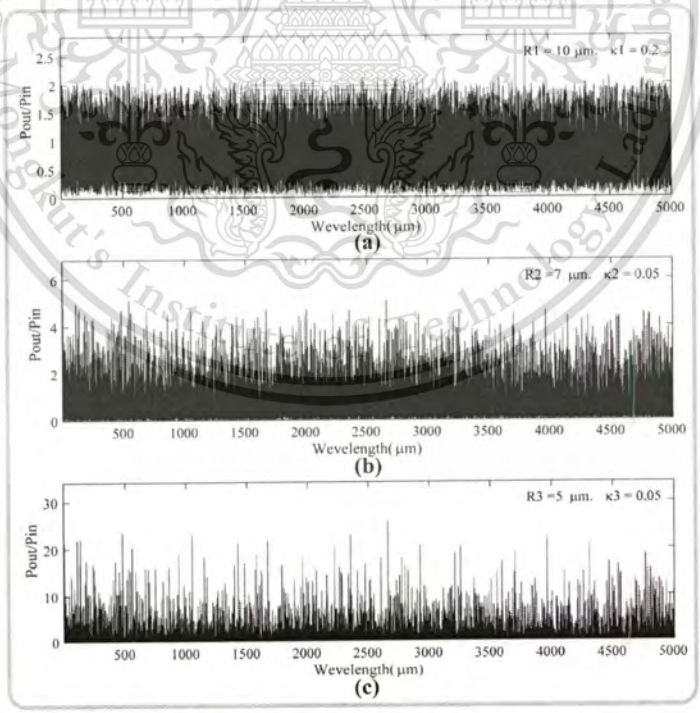


**Fig. 2.9.** Results obtained when a bring soliton pulse is input into a micro ring resonator system for

within NRR.

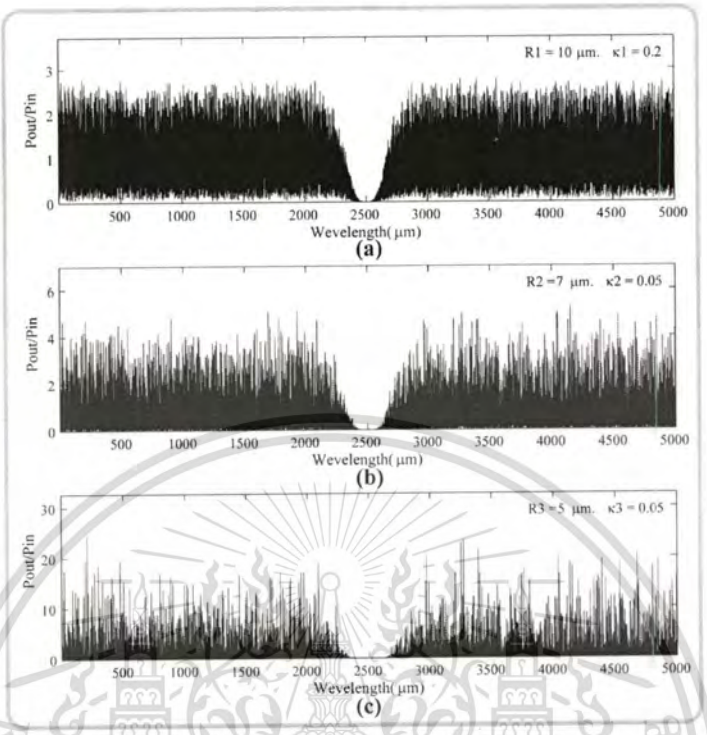


**Fig. 2.10.** Results obtained when a drak soliton pulse is input into a micro ring resonator system for within NRR.

In operation, more amplification can be obtained by using the nanoring resonator instead of the microring resonator. The results obtained for the amplification effect of dark soliton depends on the system consisting of the parameters in Fig. 2.10. In principle, the dark soliton amplification can also be employed.

#### 2.3.2.2 Dark-Bright Soliton Conversion

In operation, a dark soliton pulse with 50 ns pulse width, the maximum power of 1.0 W is input into the dark-bright solitons conversion system as shown in Fig. 2.11.

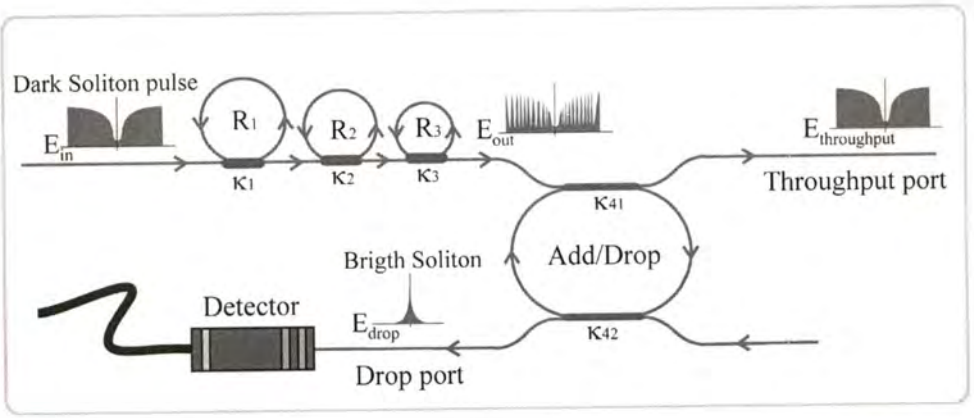


**Fig. 2.11.** A schematic of a dark-bright soliton conversion system, where $R_s$: ring radii, $\kappa_s$: coupling coefficients, $\kappa_{41}$ and $\kappa_{42}$ are the add/drop coupling coefficients.

The suitable ring parameters are used, for instance, ring radii $R_1$= 10.0 μm, $R_2$= 7.0 μm, and $R_3$= 5.0 μm. In order to make the system associate with the practical device, the selected parameters of the system are fixed to $\lambda_0$ = 1.55 μm, $n_0$ = 3.34 (InGaAsP/InP), $A_{eff}$ = 0.50, 0.25 $\mu m^2$ and 0.10 $\mu m^2$ for a micro ring and nano ring resonator, respectively, $\alpha$ = 0.5 $dBmm^{-1}$, $\gamma$ = 0.1. The coupling coefficients (kappa, $\kappa$) of the micro ring resonator are ranged from 0.05 to 0.90. The nonlinear refractive index is $n_2$=2.2 x $10^{-17}$ $m^2/W$. In this case, the wave guided loss used is 0.5$dBmm^{-1}$. The input dark soliton pulse is chopped (sliced) into the smaller signals as shown in Fig. 2.12(a).

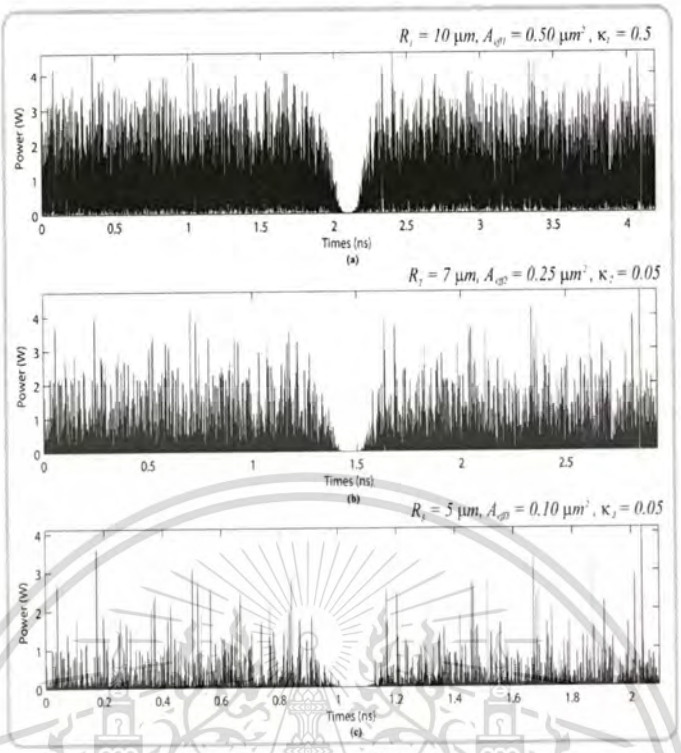


**Fig. 2.12.** Results of the soliton signals within the ring resonator system, where (a) in ring $R_1$, (b) in ring $R_2$ and (c) in ring $R_3$.

Figs.2.12(b) and 2.12(c) are the output signals of the filtering signals within the rings $R_2$ and $R_3$. We find that the output signals from $R_3$ are smaller than from $R_1$, which is more difficult to detect when it is used in the link. In fact, the multistage ring system is proposed due to the different core effective areas of the rings in the system, where the effective areas can be transferred form 0.50 $\mu m^2$ to 0.10 $\mu m^2$ with some losses. The soliton signals in $R_3$ is entered in the add/drop filter, where the dark-bright solitons conversion can be performed by using Eqs. (2.22) and (2.23). Results obtained when a dark soliton pulse is input into a micro and nano ring resonator system as shown in Fig. 2.12. The parameters used are the same as in Fig. 2.10, where the only change is the add/drop filter parameters. It is formed by two couplers and a ring radius ($R_d$) of 10 $\mu m$, the coupling constants ($\kappa_{11}$ and $\kappa_{12}$) are the same values (0.50). When the add/drop filter is connected to the third ring ($R_3$), the dark-bright solitons conversion are seen. The bright soliton and dark solitons are detected by the through (throughput) and drop ports as shown in Fig.2.13, respectively.

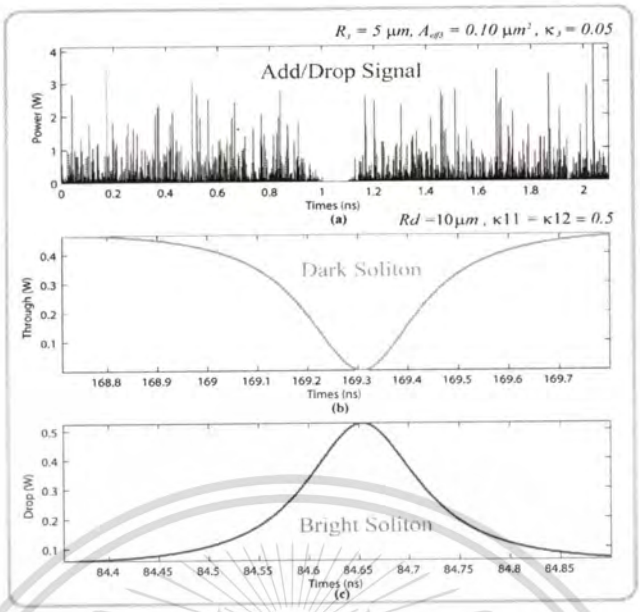


**Fig. 2.13.** Results of the optical solitons, where (a) the signals in R3, (b) a dark soliton and (c) a bright soliton.the input dark soliton power is 1 W, $\kappa_1 = 0.5$, $R_d = 10\ \mu m$.

The propagating dark soliton in the optical media can be converted to be a bright soliton by using the ring resonator system incorporating the add/drop multiplexer. By using the reasonable dark soliton input power, the output bright soliton power obtained can be used to perform the common soliton for long distance link. The advantage is that the detection of the dark soliton along the through port(transmission line) is difficult, while the detection of the bright one (by the specific user) can be performed by the standard form. This means that the use of dark soliton to form the signal security or communication security is plausible, which is also available for network security application.

# CHAPTER 3

# SENSING MODEL USING COINCIDENCE DARK-BRIGHT SOLITON PAIR

In this chapter, we present the novel concept of the interesting results by using the dark and bright solitons in a Mach Zhender interferometer (MZI), in which the coincidence dark and bright soliton pulses can establish the phase shift after entering into the MZI ports, which they are affected by the external disturbance (i.e. applied physical parameters), whereas the measurement can be performed by the signals between sensing and reference units, which can be provided the required measurements. The advantage of the proposed system is that the multi functions in terms of phase shift sensor, orthogonal soliton (entangled photon) sensor, single photon sensor and self calibration measurement can be provided, which will be discussed in the following section.

## 3.1 Introduction

Optical sensors have been implemented and widely used in various applications, for instance, in medicine, microbiology, communication, particle physics, automotive, environmental safety and defense [27-30]. Till date, the searching of new techniques of sensing devices and systems remains. Recently, the use of micro device known as a microring resonator has shown the potential applications in many area of applications [24,31], in which one of the interesting behaviors is that the use of dark-bright soliton conversion within the microring device has been proposed [3, 32]. The key interpretation is that the random output of both solitons can be separated and observed when the dark-bright soliton pair is propagated through a ($\pi$/2) phase retarder, for instance, an optical coupler or beam splitter. Hence, the dark and bright solitons are the orthogonal pulses and can be recognized as an entangled photon pair, in which the change in phase between dark and bright solitons can be recovered by using the phase shifter/controller, therefore, the measurement of the shift in phase of soliton pair can recover and perform the measurement.

## 3.2 Coincidence Dark-Bright Soliton in MZI

Dark and bright solitons are the short optical pulses that can propagate into the optical medium for long period of time with constant amplitude due to their nonlinear properties, for instance, self phase and cross phase modulations [33]. The lack of phase with ($\pi$/2) between dark and bright solitons can be used to form the orthogonal photon components (entangled photon). More details of dark and bright soliton generation and behaviors can be found in either theory or experiment in the references [34-36].

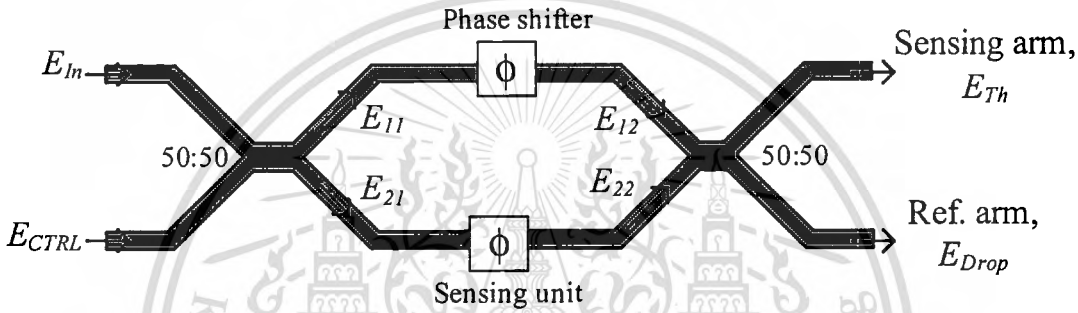


**Fig. 3.1.** A schematic of a multi function sensors.

When the dark and bright soliton pulses are generated and input into the system, the optical fields propagate through the MZI are expressed by Eqs. (3.1) – (3.3).

$$E_{11} = \frac{1}{2} In + j\frac{1}{2} A$$
$$E_{21} = \frac{1}{2} A + j\frac{1}{2} In \qquad (3.1)$$

$$E_{12} = E_{11} e^{-j\phi}$$
$$E_{22} = E_{21} e^{-\frac{\alpha}{2} L_1} \qquad \text{.....} \qquad (3.2)$$

$$Th = \frac{1}{2} E_{12} + j\frac{1}{2} E_{22}$$
$$Drop = \frac{1}{2} E_{22} + j\frac{1}{2} E_{12} \qquad (3.3)$$

where $E_{in}$ is an input field, $E_{CTRL}$ ($E_{add}$) is an added field (control), $E_{11}$ and $E_{21}$ are fields split into two arms of MZI passing through the first coupler as shown in Fig. 3.1. $E_{12}$ and $E_{22}$ are optical fields before merging into the second coupler. Throughput and drop are the output field signals. The MZI dimension can be ranged from micrometer to few meters.

We are looking for the stationary dark and bright soliton pulses, which are introduced into the MZI ports as shown in Fig. 3.1. The input optical fields, $E_{in}$ and $E_{add}$, of the dark and bright solitons, respectively, are given by [33, 36]

$$E_{in}(t) = A\tanh\left[\frac{T}{T_0}\right]\exp\left[\left(\frac{z}{2L_D}\right) - j\omega_0 t\right],$$
$$E_{add}(t) = A\,\mathrm{sech}\left[\frac{T}{T_0}\right]\exp\left[\left(\frac{z}{2L_D}\right) - j\omega_0 t\right], \tag{3.4}$$

where A and z are the optical field amplitude and propagation distance, respectively. T is a soliton pulse propagation time in a frame moving at the group velocity, $T=t-\beta_1 z$, where $\beta_1$ and $\beta_2$ are the coefficients of the linear and second-order terms of Taylor expansion of the propagation constant. $L_D = T_0^2/|\beta_2|$ is the dispersion length of the soliton pulse. $T_0$ in equation is a soliton pulse propagation time at initial input (or soliton pulse width), where t is the soliton phase shift time, and the frequency shift of the soliton is $\omega_0$. This solution describes a pulse that keeps its temporal width invariance as it propagates, and thus is called a temporal soliton. When a soliton peak intensity $|\beta_2/\Gamma T_0^2|$ is given, then $T_0$ is known. For the soliton pulse in the MZI device, a balance should be achieved between the dispersion length ($L_D$) and the nonlinear length ($L_{NL}=1/\Gamma\Phi_{NL}$), where $\Gamma=n_2k_0$, is the length scale over which dispersive or nonlinear effects makes the beam become wider or narrower. For a soliton pulse, there is a balance between dispersion and nonlinear lengths, hence $L_D = L_{NL}$.

### 3.3 Multi Function Sensors

Here, the coincident dark and bright solitons are randomly input into the MZI ports as shown in Fig. 3.1. The soliton pair is split into each branches of a MZI, where one arm is placed as a sensing unit, where the other is a phase shifter. The change in phase of both signals (solitons) is affected to the coincident dark-bright soliton pair before reaching the second coupler, in which the phase shift recovery can be employed to compensate and bring back the signals at the throughput and drop ports to the reference position. By using this proposal, a single photon sensor is also available when the soliton power is reduced to be a single photon. Moreover, the lack in phase of both solitons($\pi/2$) can establish the orthogonal solitons (entangled photons) sensor. Eventually, the shift in phase of dark and bright soliton can be compared and measured, where in addition the self calibration of phase shift between throughput and drop port signals can be operated.

In this simulation, dark and bright soliton with the center wavelength at 1.55 μm is randomly input into the MZI ports. The attenuated soliton peak power at the input coupler is 1 mW, 20 ns pulse width, and the waveguide loss of $1 dBmm^{-1}$ is included in the system (simulation).

In operation, the input field of dark soliton $|D\rangle$ or bright soliton $|B\rangle$ are input into the MZI input ports, the input fields are combined and split into two parts with the same amount via a 3dB coupler (50:50), which they are $E_{11}$ and $E_{21}$. The field $E_{12}$ is the output field of $E_{11}$ after propagating into the controlled phase shifted device.

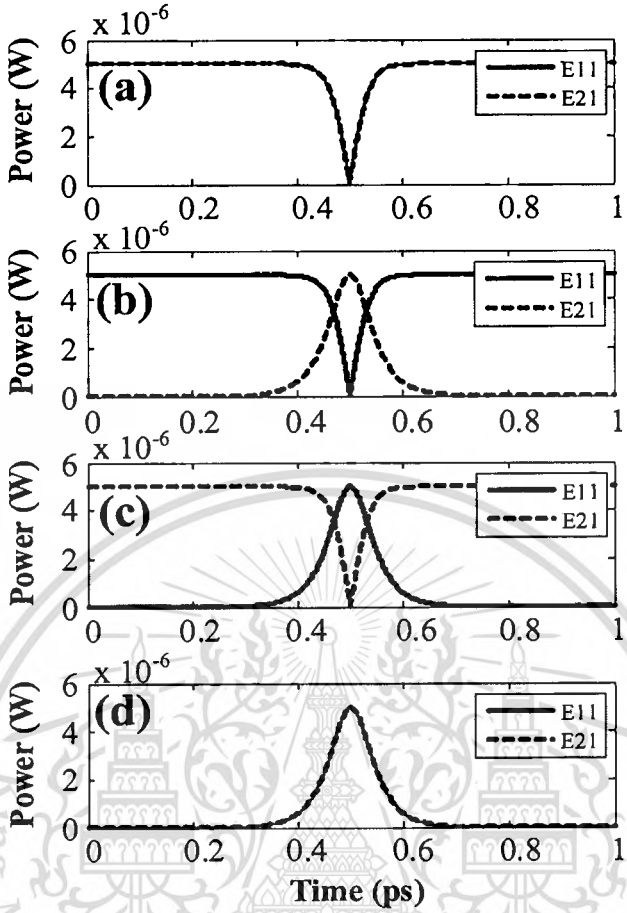


**Fig. 3.2.** Simulation results of dark and bright solitons when the input signals are (a) $|DD\rangle$, (b) $|DB\rangle$, (c) $|BD\rangle$, and (d) $|BB\rangle$.

The first dark-bright soliton conversion pulses ($E_{11}$ and $E_{21}$) are formed at the first coupler in the MZI, for instance, the obtained signals are $|DD\rangle \rightarrow |DD\rangle$, $|DB\rangle \rightarrow |DB\rangle$, $|BD\rangle \rightarrow |BD\rangle$ and $|BB\rangle \rightarrow |BB\rangle$, as shown in Fig. 3.2(a)-(d), respectively. Finally, the fields are combined again at the second 3dB coupler after the phase controlled device, in which the random combination of the orthogonal pulses (dark and bright soliton pulses) can be obtained via the MZI ports. The Throughput port output result is as shown in Fig. 3.3. From Fig. 3.3(a)-(d), the obtained signals from the throughput port are $|DD\rangle \rightarrow |BD\rangle$, $|DB\rangle \rightarrow |BB\rangle$, $|BD\rangle \rightarrow |DD\rangle$ and $|BB\rangle \rightarrow |DB\rangle$,respectively. However, the dark soliton $|D\rangle$ or bright soliton $|B\rangle$ states are required to control the phase shift by using the input fields and the phase shifter. When the phase shift device is introduced, the desired measurement of the sensing unit can be operated, in which the shift in phase of soliton pair can be compensated and brought back to the reference position.

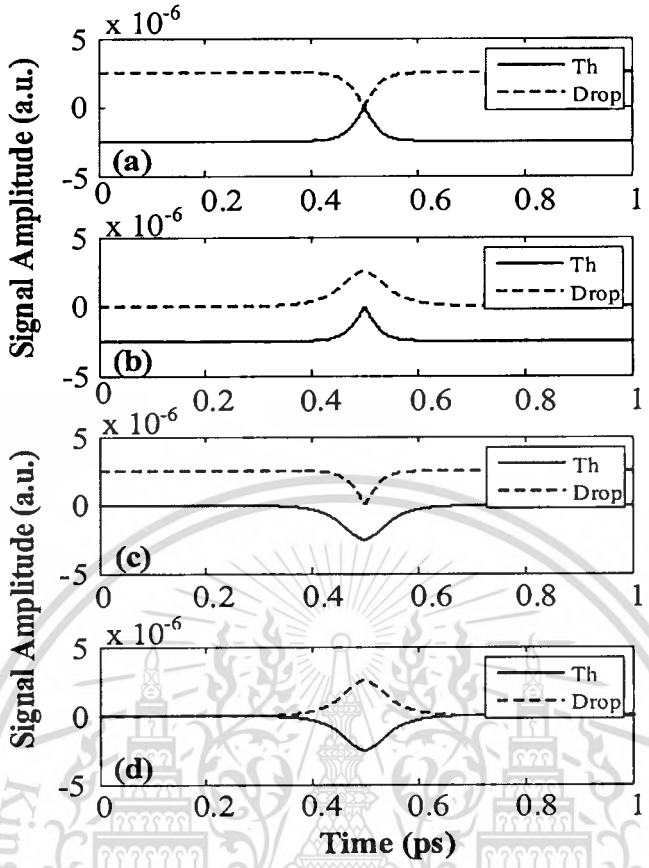


**Fig.3.3.** Simulation signals for calibration when the soliton inputs are (a) $|DD\rangle$, (b) $|DB\rangle$, (c) $|BD\rangle$, and (d) $|BB\rangle$.

Similarly, the obtained result in terms of wavelength is as shown in Fig. 3.4, the induced change in wavelength(phase) can be compared to the reference signals, the required measurement information can be obtained, where finally the measurement compensation of dark-bright soliton phase shift, orthogonal solitons, single photon can be provided. Furthermore, the self calibration between the measurement (throughput port) and reference (drop port) arms of the MZI can be functioned, which is more useful for sensing application.

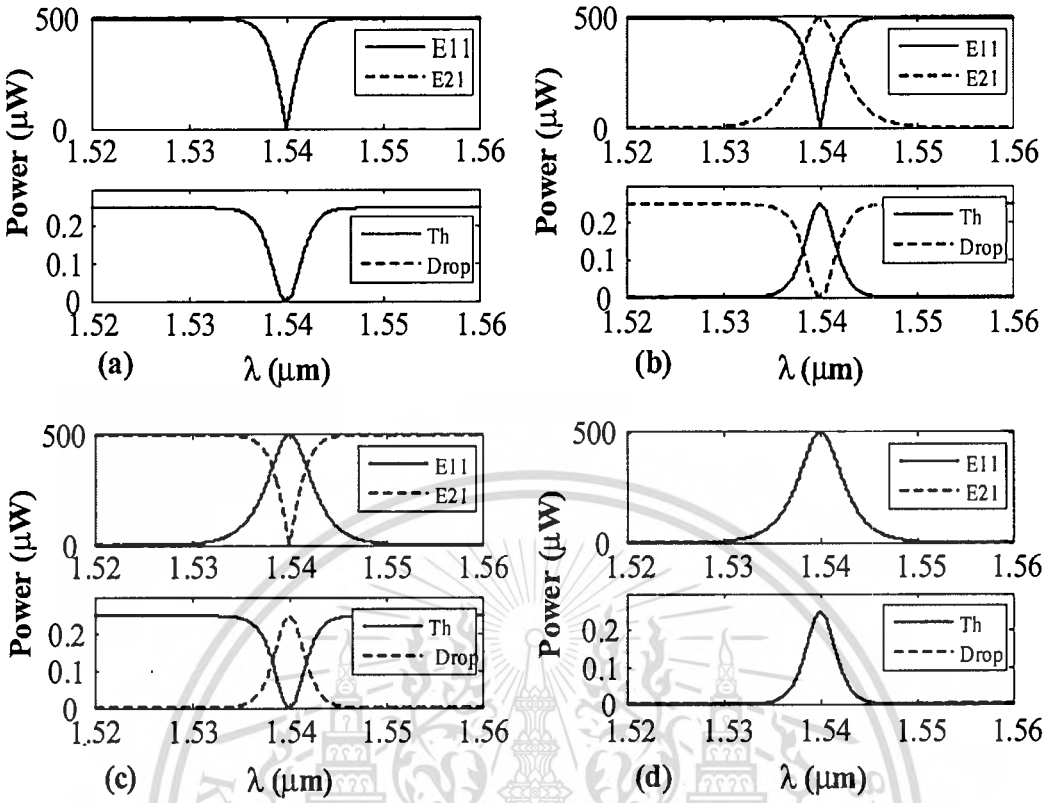


**Fig. 3.4**. Simulation signals in term of wavelengths for calibration when the soliton inputs are (a) $|DD\rangle$, (b) $|DB\rangle$, (c) $|BD\rangle$, and (d) $|BB\rangle$.

The novelty of the work is that the use of dark-bright soliton conversion to form the measurement system has never presented elsewhere. In this work, the simulation result is based on the use of practical device parameters, whereas the device fabrication to form the realistic device and application is plausible.

# CHAPTER 4

# PANDA RING RESONATOR SENSOR

In this chapter, we propose a new sensors of microring sensing transducer using a PANDA ring resonator type, in which the sensing unit is consisted of an optical add/drop filter and two nanoring resonators, where one ring is placed as a transducer (sensing unit), the other ring is set as a reference ring. In operation, the external force is assumed to exert on the sensing ring resonator. The obtained results have shown that the change in wavelength due to the change in sensing ring radii is seen, in which the wavelength shift of 1 nm resolution is achieved. The distributed sensing system is designed, which is available for network sensing applications, which are discussed in the next chapter.

## 4.1 Introduction

In the recent years, optical sensors have been implemented and widely used in various applications, for instance, in medicine, microbiology, communication, particle physics, automotive, environmental safety and defense [2,27,29]. Particularly, the integrated nonlinear optical device using a microring resonator has been widely investigated in both theory and experiment [37-39]. One of the interesting results is the use of a specific model of a ring resonator known as a PANDA ring resonator [14], which can be a good candidate for nanoscale sensing applications. The use of nanoscale measurement with more efficiency systems has been reported by several research groups [40, 41]. However, the searching system has been presented by Yupapin et al [30, 42], in which the interesting results are the self-calibration sensor base on ring resonator. Recently, the use of a new form of a ring resonator called a PANDA ring resonator has shown the interesting aspect of applications [12, 13]. The authors have shown that such a proposed form of a ring resonator can establish the new concept of dark-bright soliton collision, whereas the use of random encoding, optical vortices (tweezers) and optical/quantum gate can be generated. In this chapter, we propose the other aspect of a PANDA ring resonator, in which the system of a nano-scale sensing transducer based on a PANDA ring resonator

type is proposed. In practical the sensing ring should be free-standing. Usually, if force is applied to a free-standing structure, it is bent. Hence, the shapes of the sensing ring are deformed into an ellipse and then induce the ring circumference-shift $\Delta L$. The sensing system is functioned by mean of the change of a ring radius due to a load cell or other physical parameters, where the change in optical path length of light is caused by the same way of an interferometer [43, 44], while the other ring radius is remain constant(reference). The sensing and the reference signals are analyzed, simulated and compared. Simulation results obtained have shown that the system can be employed to be the nano-scale sensing transducer. However, the measurement limitation is occurred due to wavelength meter resolution, in which the measurement resolution of 1 nm is noted in this work. Lastly, the distributed or multiplexed sensing application is also available using the nano-scale sensing transducer via the multi wavelength router, which is discussed in details.

## 4.2 Principle and Method

To form the simulation sensing performance, the microring material used is InGaAsP/InP, with the refractive index is $n_0 = 3.34$ [45-47]. The schematic diagram of a sensing transducer using a PANDA ring resonator is as shown in Fig.4.1. The system consisted of three microring resonators, where the first ring is position as a reference ring, with radius $R_1$ = 1.550 μm. The second ring $R_2$ is the sensing ring, the radius is varied by mean of the deformation of ring radius due to an applied force or load cell, and the third ring is used to form the interference signal between reference and sensing rings, with the radius $R_3$ = 3.10 μm. In operation, the change in sensing ring radius is caused the change in the shift in signals circulated in the interferometer ring ($R_3$), in which the interference signals are seen. The change in optical path length which is related to the change of the external parameters is measured.

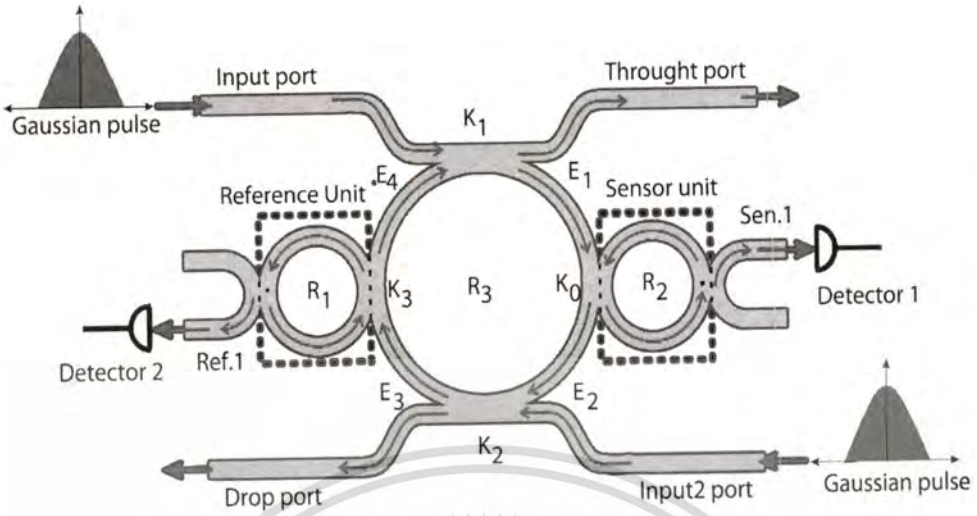


**Fig.4.1.** Schematic diagram of a nano-scale sensing transducer using a PANDA ring resonator.

Two identical beams of monochromatic optical field ($E_{in}$) of Gaussian pulse with the center wavelength 1.550 μm are launched into in the system at the input port and the add port, which is given by

$$E_{in}(t) = E_0 e^{[-\alpha L + j\phi_0(t)]} \tag{4.1}$$

where $L = 2\pi R$ is a propagation distance (waveguide length), $\alpha$ is an attenuation and $\phi_0$ is the phase constant. When light propagates within the nonlinear material (medium), by using the Kerr nonlinear effect within the ring devices, the refractive index ($n$) of light within the medium is given by

$$n = n_0 + n_2 I = n_0 + n_2\left(\frac{P}{A_{eff}}\right) \tag{4.2}$$

where $n_0$ and $n_2$ are the linear and nonlinear refractive indices, respectively. $I$ and $P$ are the optical intensity and optical power, respectively. The effective mode core area of the device is given by $A_{eff}$.

The resonance output is formed, thus, the normalized output of the light field is the ratio between the output ant input fields $[E_{th}(t)$ and $E_{in}(t)]$ in each roundtrip, which is given by [14, 37]

$$\left|\frac{E_{th}(t)}{E_{in}(t)}\right|^2 = (1-\gamma)\left[1-\frac{\left(1-(1-\gamma)x^2\right)\kappa}{\left(1-x\sqrt{1-\gamma}\sqrt{1-\kappa}\right)^2+4x\sqrt{1-\gamma}\sqrt{1-\kappa}\sin^2\left(\frac{\phi}{2}\right)}\right] \quad (4.3)$$

The optical output of ring resonator add/drop filter for the through and drop ports can be given by Eqs. (4.4) and (4.5), respectively [14]

$$\left|\frac{E_{t1}}{E_{in}}\right|^2 = \frac{(1-\kappa_1)-2\sqrt{1-\kappa_1}.\sqrt{1-\kappa_2}.e^{\frac{-\alpha}{2}L}\cos(k_nL)+(1-\kappa_2)e^{-\alpha L}}{1+(1-\kappa_1)(1-\kappa_2)e^{-\alpha L}-2\sqrt{1-\kappa_1}.\sqrt{1-\kappa_2}e^{\frac{-\alpha}{2}L}\cos(k_nL)} \quad (4.4)$$

$$\left|\frac{E_{t2}}{E_{in}}\right|^2 = \frac{\kappa_1\kappa_2.e^{\frac{-\alpha}{2}L}}{1+(1-\kappa_1)(1-\kappa_2)e^{-\alpha L}-2\sqrt{1-\kappa_1}.\sqrt{1-\kappa_2}e^{\frac{-\alpha}{2}L}\cos(k_nL)} \quad (4.5)$$

Where $E_{t1}$ and $E_{t2}$ represent the optical fields of the through and drop ports, respectively. $x=\exp\left(-\alpha L/2\right)$ is a roundtrip loss coefficient, $k_n=2\pi/\lambda$ is the wave propagation number in vacuum, $n_{eff}$ is an effective refractive index, $\phi=kn_{eff}L$ is the phase constant, $\gamma$ is the fractional coupler intensity loss, $\kappa$ is the coupling coefficient, and $\beta$ is a complex coefficient, The signals of both rings $R_1$ and $R_2$ are observed at the point Ref.1 $(E_{R1})$ and Sen.1 $(E_{S1})$ respectively as shown in Fig. 4.1, and the mathematical form of those signals are also analyzed, which can be expressed as

$$\left|\frac{E_{S1}}{E_{in}}\right|^2 = \left|\left[\frac{-(1-\gamma_S)\kappa_S}{1-Z_2(1-\gamma_S)(1-\kappa_S)}\right]\left[\frac{j.Z_3\sqrt{(1-\gamma_C)\kappa_C}\left(1+Z_3^2\beta_1\sqrt{(1-\gamma_C)(1-\kappa_C)}\right)}{1-Z_3^4\beta_1\beta_2(1-\gamma_C)(1-\kappa_C)}\right]\right|^2 \quad (4.6)$$

$$\left|\frac{E_{R1}}{E_{in}}\right|^2 = \left|\left[\frac{-(1-\gamma_R)\kappa_R}{1-Z_1(1-\gamma_R)(1-\kappa_R)}\right]\left[\frac{j.Z_3\sqrt{(1-\gamma_C)\kappa_C}\left(1+Z_3^2\beta_2\sqrt{(1-\gamma_C)(1-\kappa_C)}\right)}{1-Z_3^4\beta_1\beta_2(1-\gamma_C)(1-\kappa_C)}\right]\right|^2 \quad (4.7)$$

Where $E_{S1}$ and $E_{R1}$ represent the sensing and reference signal respectively, $\gamma_S = \gamma_0$ and $\gamma_R = \gamma_3$ are the fractional coupler intensity loss in sensing and reference unit, $\kappa_S = \kappa_3$ and $\kappa_R = \kappa_0$ are the coupling coefficient in sensing and reference unit, $Z_1 = \exp\left(\frac{-\alpha}{8}\frac{L_1}{2} - jk_n\frac{L_1}{2}\right)$, $Z_2 = \exp\left(\frac{-\alpha}{8}\frac{L_2}{2} - jk_n\frac{L_2}{2}\right)$ and $Z_3 = \exp\left(\frac{-\alpha}{8}\frac{L_3}{4} - jk_n\frac{L_3}{4}\right)$ are loss coefficients, and $\beta$ is a complex coefficient, which they are described by

$$\beta_1 = \left[\frac{\sqrt{(1-\gamma_3)(1-\kappa_3)} + (1-\gamma_3).e^{\frac{-\alpha L_1}{4} - jk_n L_1}}{1 - \sqrt{(1-\gamma_3)(1-\kappa_3)}.e^{\frac{-\alpha L_1}{4} - jk_n L_1}}\right] \tag{4.8}$$

$$\beta_2 = \left[\frac{\sqrt{(1-\gamma_0)(1-\kappa_0)} + (1-\gamma_0).e^{\frac{-\alpha L_2}{4} - jk_n L_2}}{1 - \sqrt{(1-\gamma_0)(1-\kappa_0)}.e^{\frac{-\alpha L_2}{4} - jk_n L_2}}\right] \tag{4.9}$$

The power output $P$ at all ports is expressed by

$$P = |E|^2 \tag{4.10}$$

For common sensing applications such as bio/chemical sensing, the interaction between molecules and sensing layer leads to change in refractive index in the layer. Consequently, the light mode supported by the ring resonator experiences this change through its evanescent field, leading to change in effective index [44]. This, in turn, results in shift in resonance wavelength of the mode. Employing Eqs. (4.11), in general, the shift in resonant wavelength with effective index and physical dimension change is given by:

$$\frac{\Delta\lambda}{\lambda} = \frac{\Delta n}{n} + \frac{\Delta L}{L} \tag{4.11}$$

The first contribution for the shift in resonance is the change in $n$ which actually changes when the refractive index on the surface of the ring is modified by the interaction of analytes with sensing layer. Any mechanical effect leading to the change in the size of the ring structure could also modify the optical mode in the resonator and hence leading to a shift in the resonance wavelength. However, first contribution does not apply to our structure, thus the first term on the right side of the above equation can be ignored.

### 4.3 Sensor based on a PANDA Ring Resonator

In simulation, the sensing ring circumference $L_2$ is varied, in which the optical path length is also changed, and an interferometer system is formed [43, 48]. In practical if the sensing unit is coupling with other surrounding things such as DNA or molecule, so the external force was applied to the sensing unit, then the sensing unit will be deform, say in ellipse or oval shape, and then it is also cause the changed in circumference, which the ellipse circumference can be explained by Eq. (4.12).

$$L_{ellipse} = \frac{\pi}{2}\left[3(a+b) - \sqrt{(3a+b)(a+3b)}\right] \tag{4.12}$$

Where $a$ and $b$ are semi-major and semi-minor axis respectively.

To compare the reference and sensing signals, we set $\gamma_0 = \gamma_3$, $\kappa_0 = \kappa_3$ so $\beta_1 = \beta_2$ and then set $\gamma_S = \gamma_R$, where finally $E_{S1}$ and $E_{R1}$ are both identical, if $L_1 = L_2$. Then $E_{S1}$ is varied while $L_2$ is changed by mean of varying $R_2$ with respect to $E_{R1}$, in which $R_2$ remains constant. The change in optical path length between sensing and reference signals are compared by the use of MATLAB programming, in which the induced change by the external parameters is measured. To confirm the results the finite difference time domain method (FDTD), is also used to analyze the signal via the computer programming called Opti-wave, whereas all the parameters are simulated based on the practical parameters. The simulation steps are 40,000 iterations and the peak spectrum at reference point and sensing point are shown Fig.4. 2.

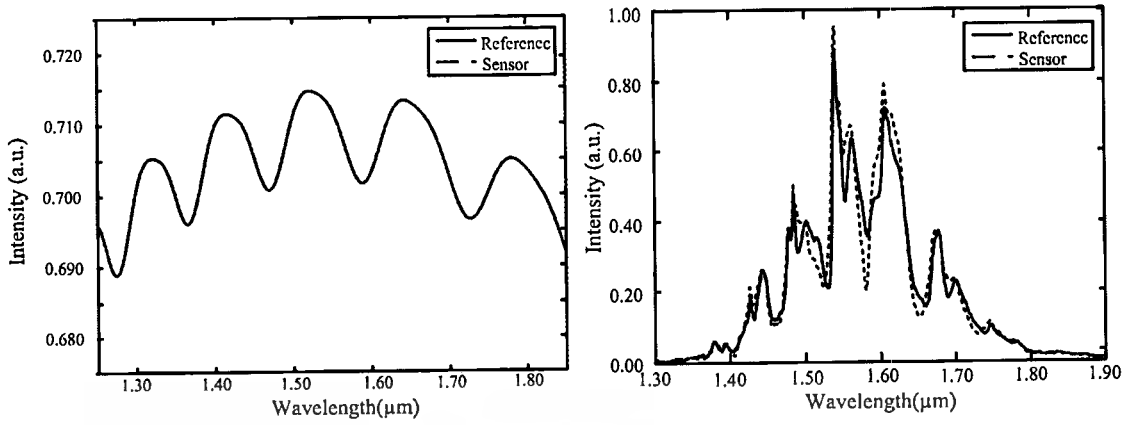


**Fig.4.2**. Shows the relationship between intensity and wavelength of sensing ( $E_{S1}$), dot red line, and reference signals ( $E_{R1}$ ), solid blue line, with $\Delta L = 0$ , obtained by (a) MATLAB and (b) Opti-wave programming.

This measurement is formed by the comparison of the shift in wavelength (optical path length), which is called ***self-calibration***, and the difference between center peak wavelengths ($\Delta\lambda$) is obtained by

$$\Delta\lambda = \lambda_2 - \lambda_1 \tag{4.13}$$

where $\lambda_1$ and $\lambda_2$ are the peak wavelengths of Ref.1 and Sen.1, respectively. The relationships between intensity and wavelength-shift are plots as shown in Fig.4.3 by MATLAB programming and Fig.4.4 by Opti-wave computer program , which is set as a self-calibration sensing transducer.

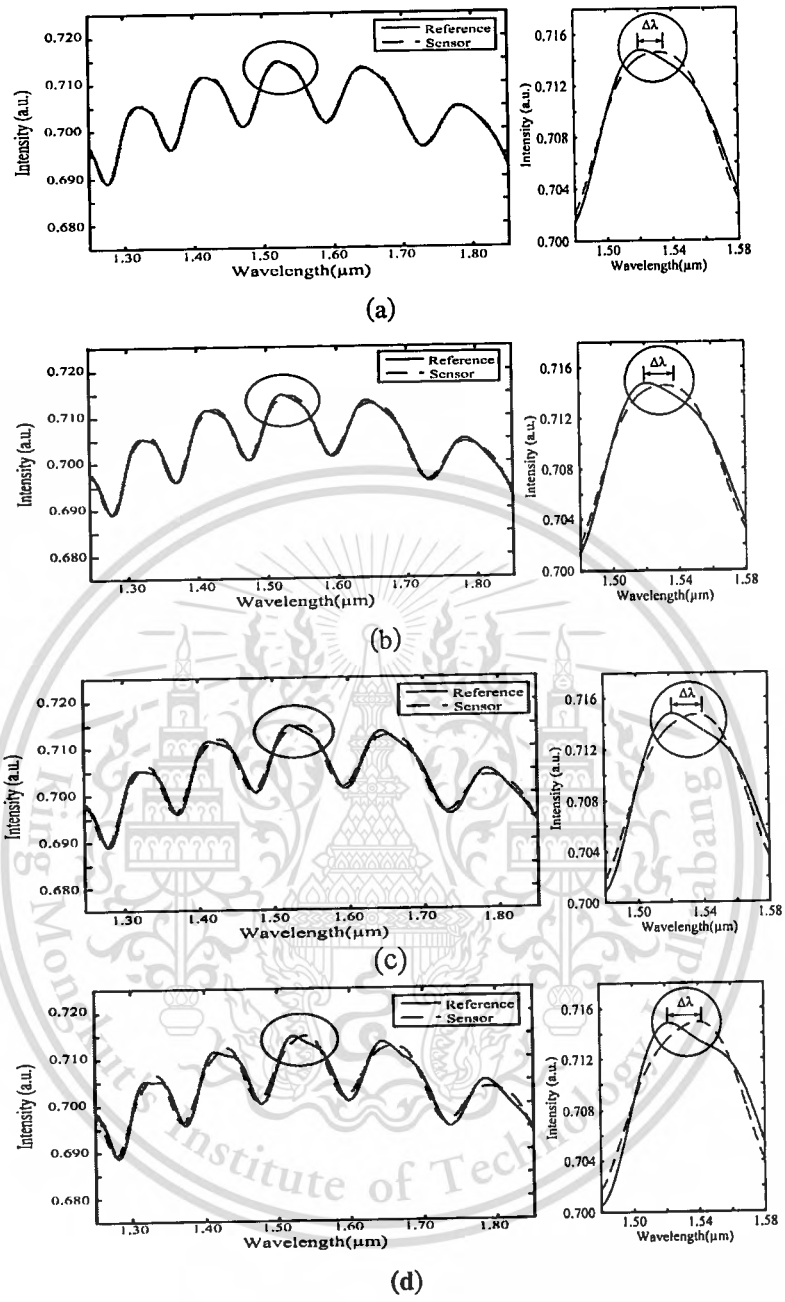


**Fig.4.3**. Shows the relationship between intensity and wavelength of sensing ($E_{SI}$), dot red line, and reference signals ($E_{RI}$), solid blue line, with the Ring Circumstance-shift, (a) $\Delta L$ = 0.01257 μm, (b) $\Delta L$ = 0.02514 μm, (c) $\Delta L$ = 0.03771 μm, and (d) $\Delta L$ = 0.05028 μm.

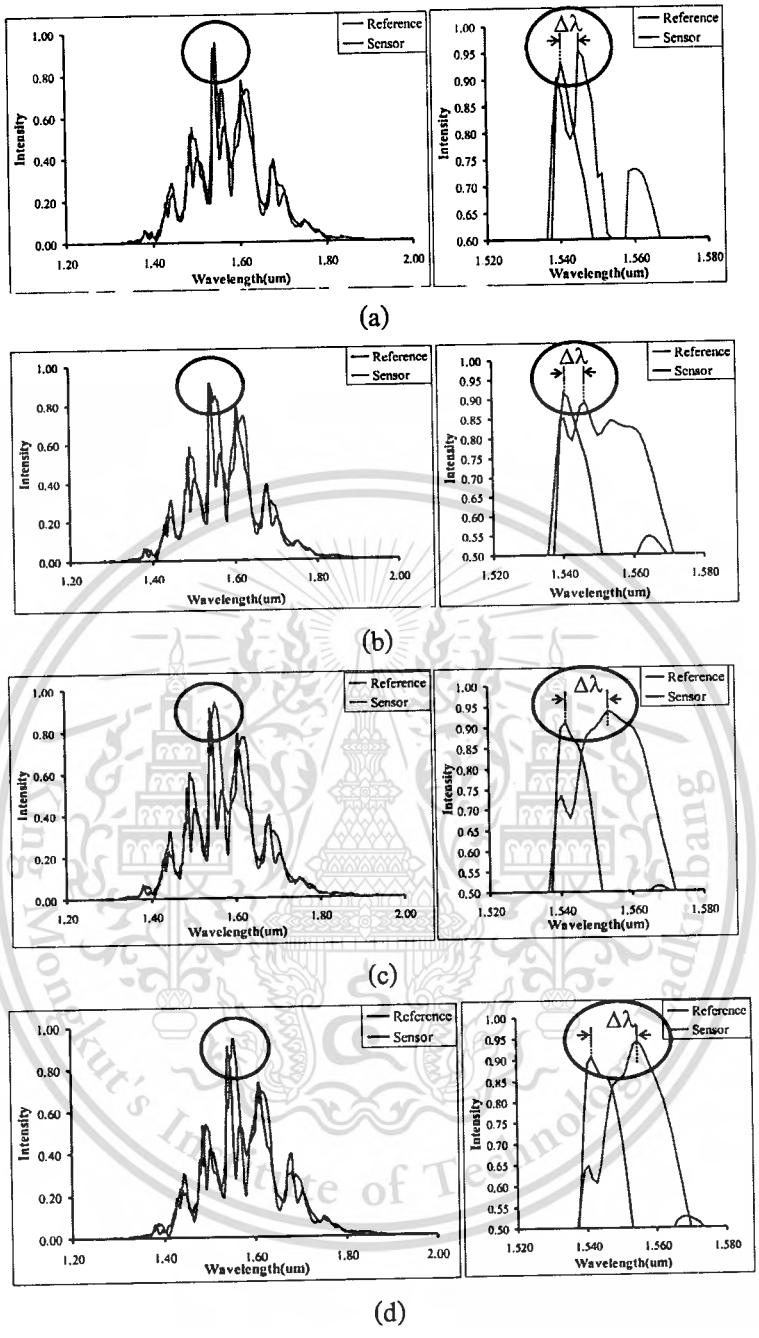


**Fig.4.4.** Shows the relationship between intensity and wavelength of sensing ($E_{SI}$) and reference signals ($E_{RI}$), with the Ring Circumstance-shift, (a) $\Delta L$ = 0.01257 μm, (b) $\Delta L$ = 0.02514 μm, (c) $\Delta L$ = 0.03771 μm, and (d) $\Delta L$ = 0.05028 μm.

Both signals, i,e, sensing and reference signals are observed and compared, and the self-calibration transducer is performed [40, 41]. We assume that the load cell or others sensing parameters is applied on the second ring $R_2$, whereas stress and strain are introduced on the sensing unit by mean of the elastic modulus of the materials. This is caused the difference in peak spectrum of both signals, which is described by the Eqs. (4.14).

$$Y_0 = \frac{F/A}{\Delta L/L} = \frac{Stress}{Strain} \tag{4.14}$$

and the relationship between force and the difference length is described by

$$F = \left(\frac{Y_0 A_0}{L_0}\right).\Delta L \tag{4.15}$$

Where $F$ is the applied force, $Y_0$ is the Young Modulus, $A_0$ is the initial cross-section area, $L_0$ is the initial length and $\Delta L$ is the difference in length. According to the properties of InGaAsP/InP material [45-47]

By using Eq. (4.6-4.15) the relationship between intensity and wavelength of the sensing signals, which calculated and simulated by MATLAB and Opti-wave programming respectively are show in Figs.4.3-4.4 and the results showed that they are corresponding in the same analogous. And the relationship between the ring circumstance-shift $\Delta L$ and wavelength shift, for both MATAB and Opti-wave programming are plotted as shown in Fig. 4.5, the linearity relationship between the $\Delta L$ and wavelength shift with $R^2$ = 0.653 is formed, which is shown in good linearity for sensing application. We found that a sensing range in terms of wavelength-shift ( $\Delta\lambda$ ) within the resolution of 1 nm is achieved. By using the least square curve fitting, the linearity relationship between the applied force and $\Delta L$ with R2 = 1.00 is formed, which is shown in the Fig. 4.6. In this case study, the applied micro/nano force ranges were given between 0.00 and 8.00 nN.

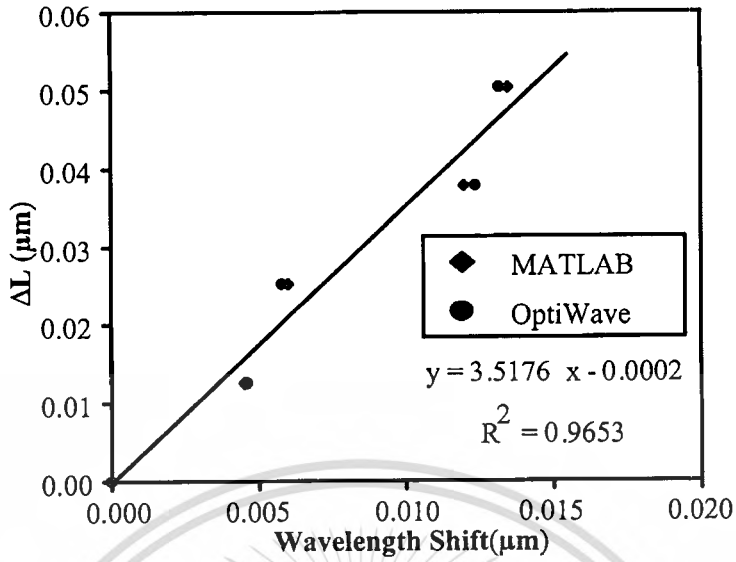


**Fig.4.5.** Graph of the linear relationship between Ring Circumstance-shift ( $\Delta L$ ) and the Wavelength-shift ( $\Delta\lambda$ ).

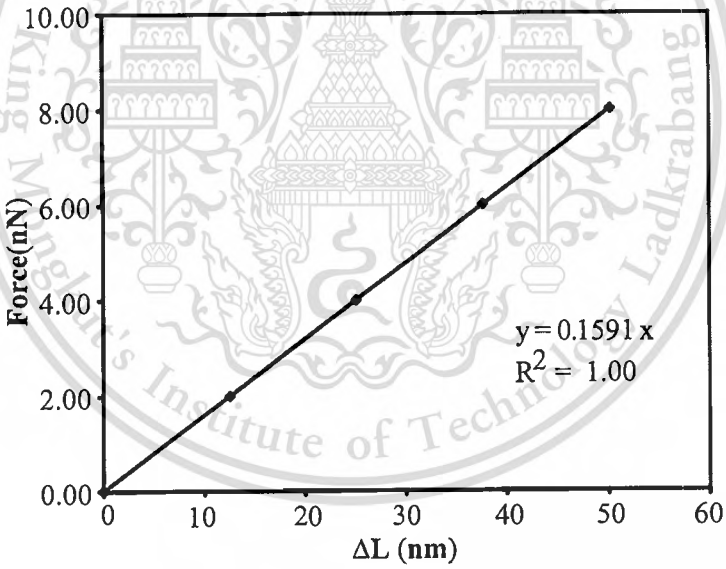


**Fig.4.6** Graph of the linear relationship between Force and the $\Delta$L.

The system have the measuring regions with in the range of 1 nm, in which the self-calibration of the measurement of two sensing and reference signal can be compared without any additional optical part or other addition unit. The calibration is allowed by using the change in wavelength between sensing and reference signals, which is existed within the system. The other advantage is that available foe network sensing applications due to the use of the integrated optic device, which has shown in the next chapter.

# CHAPTER 5

# SENSOR VIA WAVELENGTH ROUTERS

In this chapter, we propose a new system of distributed network sensors, which is available for network sensing applications. In principle, the multi wavelength router is generated by dark soliton pulses propagating within the resonator, which are allowed to form in the multi sensors (sensing transducers), which are formed by the sensing ring devices. The sensing system is suitable to perform the multi sensing measurements in the nano scale regime such as force, stress and temperature. Moreover, the distributed or multiplexed sensing applications are also available using the nano-waveguide sensing devices incorporating the array waveguide, which are discussed in details.

## 5.1 Introduction

Soliton communication has been a successful system for long distance optical communication link, where the required minimum repeater is the advantage, which becomes the key advantage of the system performance. However, in practice, the problem of soliton-soliton interaction, soliton collision and dispersion management is required to solve [49-51]. To date, several papers have investigated the dark soliton behaviors [52-56] and one of them shows an interesting result that the dark soliton can be converted into a bright soliton and finally detected. This means that the dark soliton penalty can be used as a communication security so that it can be retrieved by the dark-bright soliton conversion [8, 57]. Recently, a soliton pulse has been used to produce fast switching [4] localized within a nano-waveguide [7, 58] and it was reported that they have designed a system which consists of micro and nanoring resonators. '

Since, the dark soliton behavior has become the promising application when the transmission dark soliton can be converted into bright soliton after passing through into the specific add/drop filter [8], which means that the transmission signals can be transmitted in the form of dark soliton, which is difficult to detect, whereas the specific end user that connects to the link via the specific add/drop

filter can obtain the signals. Although, the dark soliton applications have been widely investigated in various applications [34,59-61], the searching for new techniques that can be performed more available applications remains.

## 5.2 Multi Dark Solitons Generation

In this case, the multi dark solitons are required to form the dark soliton array in the system. To describe the multiplexed dark soliton pulses, a stationary multi dark soliton pulses are introduced into the microring resonator system as shown in Fig.5.1. Each of input optical fields ($E_{in}$) of the dark soliton pulses input is given by [62]

$$E_{in}(t) = A\tanh\left[\frac{T}{T_0}\right]\exp\left[\left(\frac{z}{2L_D}\right) - i\omega_0 t\right] \tag{5.1}$$

Where A and z are the optical field amplitude and propagation distance, respectively. T is a soliton pulse propagation time in a frame moving at the group velocity, $T = t - \beta_1 * z$, where $\beta_1$ and $\beta_2$ are the coefficients of the linear and second-order terms of Taylor expansion of the propagation constant. $L_D = T_0^2/|\beta_2|$ is the dispersion length of the soliton pulse. $T_0$ in equation is a soliton pulse propagation time at initial input (or soliton pulse width), where t is the soliton phase shift time, and the frequency shift of the soliton is $\omega_0$. This solution describes a pulse that keeps its temporal width invariance as it propagates, and thus is called a temporal soliton. When a soliton peak intensity ($|\beta_2/\Gamma \times T_0^2|$) is given, then $T_0$ is known. For the soliton pulse in the microring device, a balance should be achieved between the dispersion length ($L_D$) and the nonlinear length ($L_{NL} = 1/\Gamma\phi_{NL}$), where $\Gamma = n_2 * k_0$, is the length scale over which dispersive or nonlinear effects makes the beam become wider or narrower. For a soliton pulse, there is a balance between dispersion and nonlinear lengths, hence $L_D = L_{NL}$.

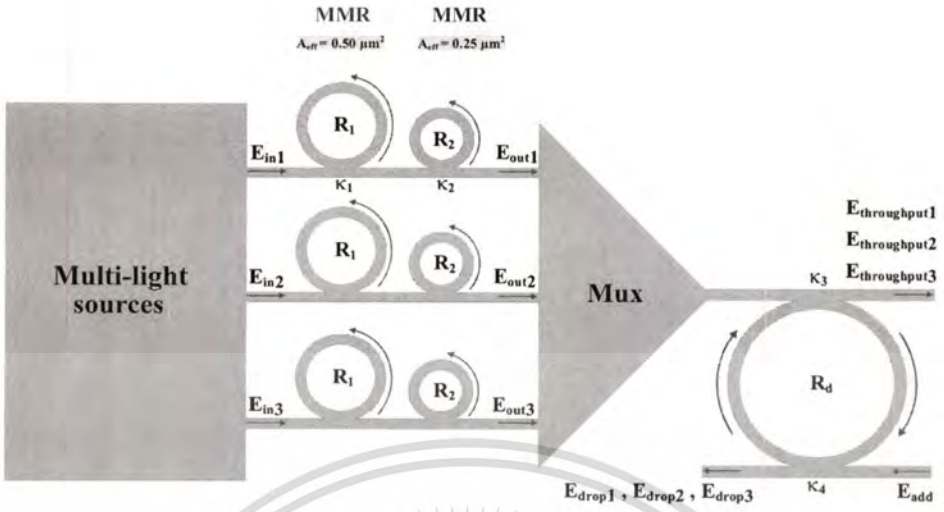


**Fig.5.1.** Schematic of dark soliton array generation, where $E_{ins}$: Soliton inputs, $R_s$: Ring radii, $\kappa_s$: Coupling coefficients, MUX: Optical multiplexer, $R_d$: Add/drop radius, MRR: Microring resonator.

When light propagates within the nonlinear material (medium), the refractive index (n) of light within the medium is given by

$$n = n_0 + n_2 I = n_0 + \frac{n_2}{A_{eff}} P \tag{5.2}$$

where $n_0$ and $n_2$ are the linear and nonlinear refractive indexes, respectively. I and P are the optical intensity and optical power, respectively. The effective mode core area of the device is given by $A_{eff}$. For the series microring resonator (MRRs), the effective mode core areas range from 0.50 to 0.10 $\mu m^2$ [19]. When a soliton pulse is input and propagated within a MRR, as shown in Fig.xx.1, which consists of a series MRRs. The resonant output is formed, thus, the normalized output of the light field is the ratio between the output and input fields [$E_{out}(t)$ and $E_{in}(t)$] in each roundtrip, which is given by [22]

$$\left|\frac{E_{out}(t)}{E_{in}(t)}\right|^2 = (1-\gamma)\left[1-\frac{(1-(1-\gamma)x^2)\kappa}{(1-x\sqrt{1-\gamma}\sqrt{1-\kappa})^2+4x\sqrt{1-\gamma}\sqrt{1-\kappa}\sin^2(\frac{\varphi}{2})}\right] \quad (5.3)$$

The close form of Eq. (5.3) indicates that a ring resonator in this particular case is very similar to a Fabry–Perot cavity, which has an input and output mirror with a field reflectivity, (1−κ), and a fully reflecting mirror. κ is the coupling coefficient, and x=exp(−αL/2) represents a roundtrip loss coefficient, $\phi_0=kLn_0$ and $\phi_{NL}=kLn_2|E_{in}|^2$ are the linear and nonlinear phase shifts, $k=2\pi/\lambda$ is the wave propagation number in a vacuum, where L and α are waveguide length and linear absorption coefficient, respectively. In this work, the iterative method is introduced to obtain the results as shown in Eq. (5.3), and similarly, when the output field is connected and input into the other ring resonators.

The input optical field as shown in Eq. (5.1), i.e. a dark soliton pulse, is input into a nonlinear series micro ring resonator. By using the appropriate parameters, we propose to use the add/drop device with the appropriate parameters. This is given in details as followings. The optical outputs of a ring resonator add/drop filter can be given by the equations (5.4) and (5.5), respectively [21].

$$\left|\frac{E_t}{E_{in}}\right|^2 = \frac{(1-\kappa_1)-2\sqrt{1-\kappa_1}\cdot\sqrt{1-\kappa_2}e^{-\frac{\alpha}{2}L}\cos(k_nL)+(1-\kappa_2)e^{-\alpha L}}{1+(1-\kappa_1)(1-\kappa_2)e^{-\alpha L}-2\sqrt{1-\kappa_1}\cdot\sqrt{1-\kappa_2}e^{-\frac{\alpha}{2}L}\cos(k_nL)} \quad (5.4)$$

And

$$\left|\frac{E_d}{E_{in}}\right|^2 = \frac{\kappa_1\kappa_2 e^{-\frac{\alpha}{2}L}}{1+(1-\kappa_1)(1-\kappa_2)e^{-\alpha L}-2\sqrt{1-\kappa_1}\cdot\sqrt{1-\kappa_2}e^{-\frac{\alpha}{2}L}\cos(k_nL)} \quad (5.5)$$

where $E_t$ and $E_d$ represent the optical fields of the throughput and drop ports, respectively. $\beta = kn_{eff}$ is the propagation constant, $n_{eff}$ is the effective refractive index of the waveguide, and the circumference

of the ring is $L=2\pi R$, with R as the radius of the ring. In the following, new parameters is used for simplification with $\phi = \beta L$ as the phase constant. The chaotic noise cancellation can be managed by using the specific parameters of the add/drop device, and the required signals can be retrieved by the specific users. $\kappa_1$ and $\kappa_2$ are the coupling coefficient of the add/drop filters, $k_n=2\pi/\lambda$ is the wave propagation number for in a vacuum, and where the waveguide (ring resonator) loss is $\alpha$ = 0.5 $dBmm^{-1}$. The fractional coupler intensity loss is $\gamma$ = 0.1. In the case of the add/drop device, the nonlinear refractive index is neglected.

## 5.3 Distributed Sensing Mechanism

The key advantage of the proposed system is the multi-soliton pulses, which is available for high performance communication, where the idea of the individual communication channel occupation is plausible. Since, a soliton communication has been recognized as a good candidate for long distance communication, therefore, the increasing in more soliton channels (wavelengths) is interesting. In this work, we demonstrate that a soliton pulse has the interesting characteristics when propagating in the nolinear micro ring device.

In simulation, the generated dark soliton pulse, for instance, with 50-ns pulse width, and a maximum power of 0.5W is input into each of ring resonator systems with different center wavelengths, as shown in Fig. 5.1. The suitable ring parameters are used, such as ring radii and ring coupling coefficients, where $R_1$=15.0μm and $R_2$=10.0μm. In order to make the system associate with the practical device [19], $n_0$=3.34 (InGaAsP/InP). The effective core areas are $A_{eff}$=0.50 and 0.25 $\mu m^2$ for MRRs. The waveguide and coupling loses are $\alpha$ =0.5 $dBmm^{-1}$ and $\gamma$ =0.1, respectively, and the coupling coefficients $\kappa_s$ of the MRRs are ranged from 0.03 to 0.1. The nonlinear refractive index is $n_2=2.2\times10^{-13}$ $m^2/W$. In this case, the waveguide loss used is 0.5 $dBmm^{-1}$. However, more parameters are used as shown in Fig. 5.1. The input dark soliton pulse is chopped (sliced) into the smaller signals $R_1$, $R_2$, and the filtering signals within add/drop ring $R_d$ are seen. We find that the output signals from $R_2$ is larger than from $R_1$ due to the different core effective areas of the rings in the system, however, the effective areas can be transferred from 0.50 and 0.25$\mu m^2$ with some losses. The soliton signals in $R_d$ is entered in the add/drop filter, where the dark soliton conversion can be performed by using Eqs. (5.4) and (5.5). In application, the different dark soliton wavelength is input into the series microring

resonators system, whereas the parameters of system are set the same. For instance, the dark solitons are input into the system at the center wavelengths $\lambda_1 = 1.5$, $\lambda_2 = 1.52$ and $\lambda_3 = 1.54$ μm, respectively. When a dark soliton propagates into the MRRs system, the occurrence of dark soliton collision (modulation) in multiplexer system and the filtering signals within add/drop ring (Rd) is as shown in Fig. 5.1. The dark soliton generated by multi-light sources at the center wavelength $\lambda_1 = 1.5$ μm, the filtering signals are as shown in Fig. 5.2. Simulation results obtained have shown that the band of bright solitons is seen, whereas there is no signal at $\lambda_1 = 1.5$μm. The free spectrum range (FSR) and the amplified power of 2.1 nm and 20 W of the dark soliton are obtained, where in this case, the spectral width(Full width at half maximum, FWHM) of 0.1 nm is achieved. In Fig.5.3, the dark soliton array generated by multi-light sources at the center wavelength $\lambda_1 = 1.5$, $\lambda_2 = 1.52$ and $\lambda_3 = 1.54$ μm and filtering signals is shown, respectively. Similarly, the dark soliton array generated by multi-light sources at the center wavelength $\lambda_1 = 1.56$, $\lambda_2 = 1.58$ and $\lambda_3 = 1.60$ μm and filtering signals respectively is as shown in Fig. 5.4, whereas the optical ring radii used are 15, 10 μm and $R_d = 50$ μm.

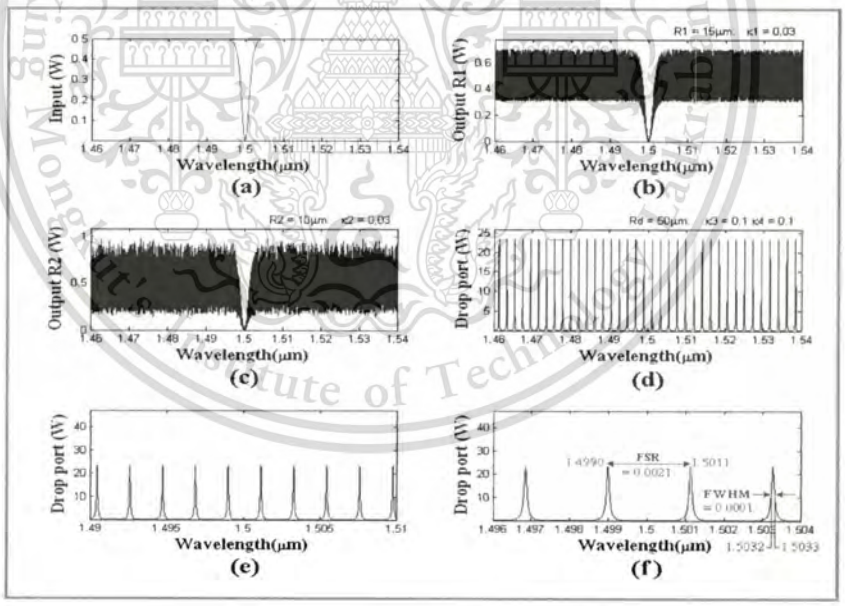


**Fig.5.2.** Simulation result of the dark solitons within the series microring resonators when the dark soliton input wavelength is 1.5 μm, where (a) dark soliton input, (b) and (c) dark solitons in Rings $R_1$ and $R_2$,(d), (e) and (f) are drop port signals.

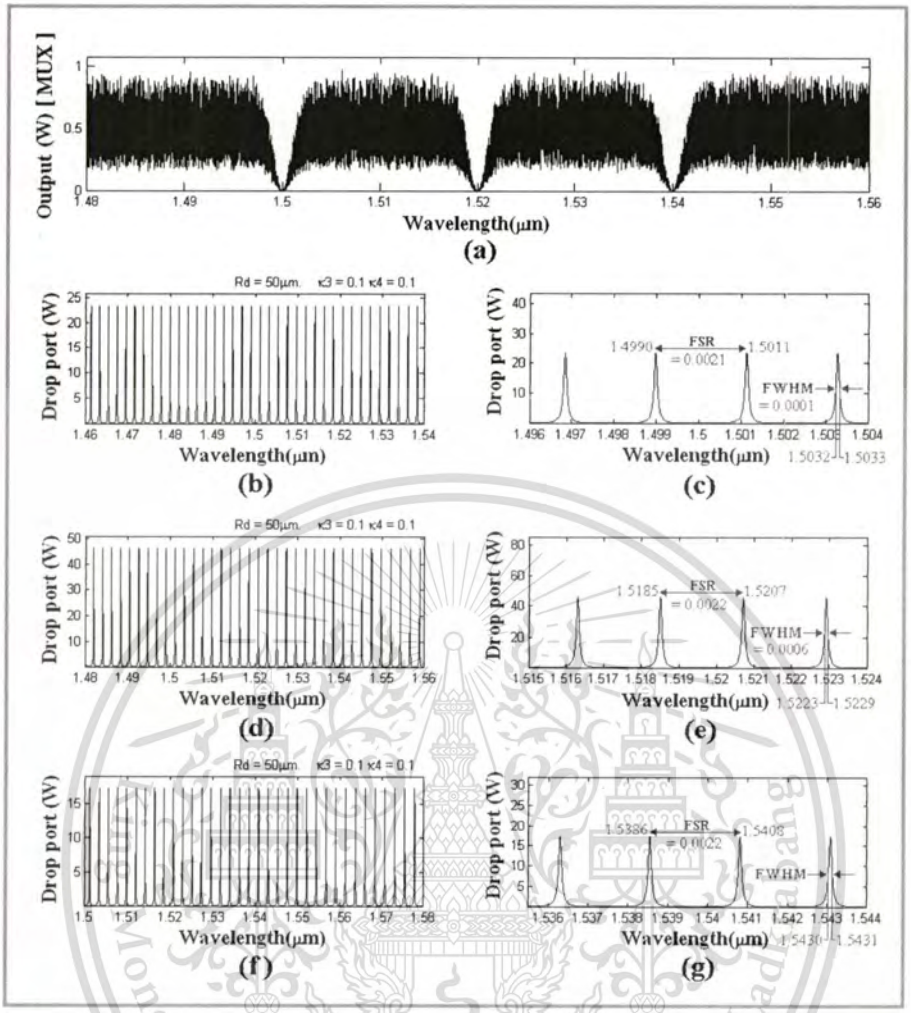


**Fig.5.3.** Simulation result of the dark soliton array when the dark soliton input wavelengths are 1.5, 1.52 and 1.54 μm, where (a) dark soliton array, (b) and (c), (d) and (e), (f) and (g) are the drop port signals, respectively.

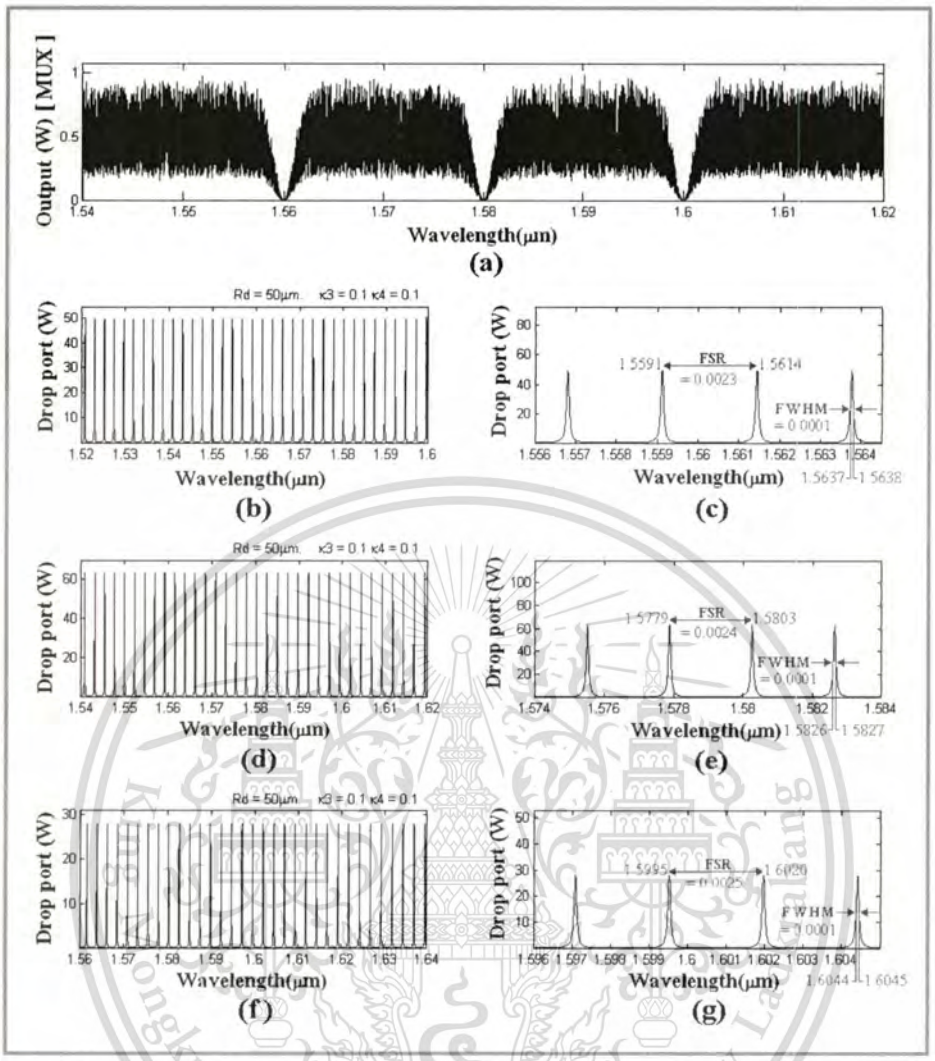


**Fig.5.4.** Simulation result of the dark soliton array when the dark soliton input wavelengths are 1.56, 1.58 and 1.60 μm, where (a) dark soliton array, (b) and (c), (d) and (e), (f) and (g) are the drop port signals, respectively.

The channel spacing of the communication signals within a wavelength router can be provided by using the suitable free spectrum range, which can be managed by using the crosstalk effect analysis. One example has shown that the multi variable network over 50 km with 40 users can be achieved , which is confirmed by Vongchumyen et al [63].

Finally, the distributed sensors (network sensors) using a PANDA ring resonator can be performed as shown in Fig.5.5, firstly, the multi dark solitons generated are input into the routers via the output/through port, which means that each sensing ring device occupies a different spatial

soliton pulse with different wavelengths ($\lambda_i$). Secondly, the sensing information can be transmitted via the network system, whereas the measurement of the change in wavelength can be performed using the PANDA ring resonator of the add/drop multiplexer, which can form the measurement of interest (force, stress or temperature). Thus, the changes in the wavelength in each wavelengths due to the change in physical parameters can be formed by the multiplexed sensors, which are the distributed network sensing system via the multi wavelength routers.

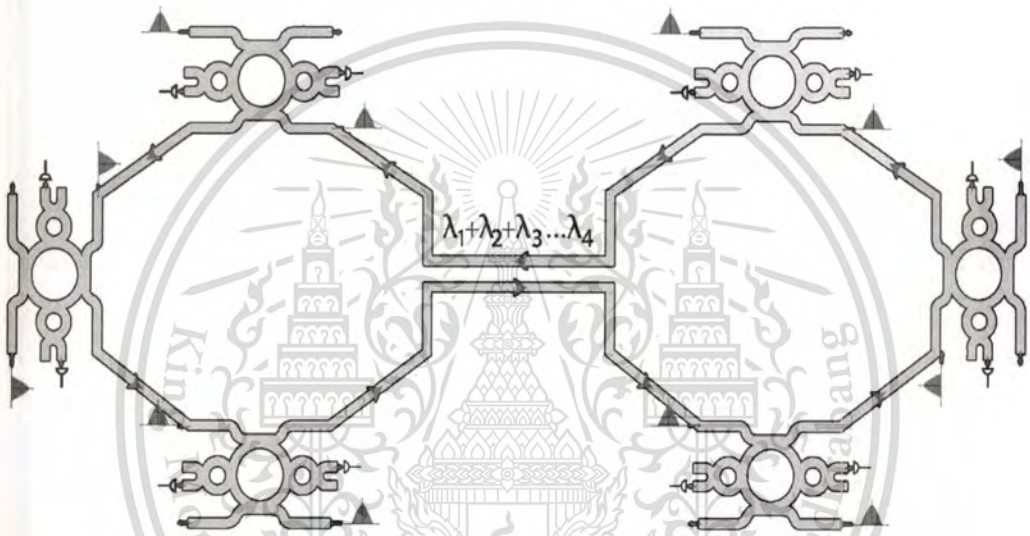


**Fig.5.5**. Schematic of a distributed network sensors system via wavelength router.

# CHAPTER 6

# CONCLUSIONS AND FUTURE WORK

A study of an optical pulse in fiber optic ring resonator have demonstrated that some interesting results can be obtained when the laser pulse is propagated within the nonlinear optical ring resonator, this can be used to perform many applications, especially, in optical communication. The propagating dark soliton in the optical media can be converted to be a bright soliton by using the ring resonator system incorporating the add/drop multiplexer. By using the reasonable dark soliton input power, the output bright soliton power obtained can be used to perform the common soliton for long distance link. The advantage is that the detection of the dark soliton along the through port (transmission line) is difficult, while the detection of the bright one (by the specific user) can be performed by the standard form. This means the use of dark soliton to form the signal security or communication security is plausible, which is also available for network security application. The dark-bright signal amplification can also be used to use in long distance communication link with security applications.

In this chapter we will conclusions the all sensors that have been proposed. In section 6.1 the new technique of multi function sensors using dark and bright solitons in a MZI. Section 6.2 the system of a nano-scale sensing transducer using PANDA ring resonator. Section 6.3 network sensor is also available due to the use of the integrated optic device via multi wavelength router. Finally, section 6.4 present recommendations for further research.

## 6.1 Sensors using Coincidence Dark-Bright Soliton Pair

We have proposed the new technique of multi function sensors using dark and bright solitons in a MZI. By using two coincidence signals of soliton pulses (Dark and Bright solitons), the orthogonal states between dark and bright soliton can establish within the system, in which the soliton states can be randomly detected at the output coupler. The change in phase of the dark and bright soliton pair away from the coincidence position, which is induced by the external disturbance can be

compensated by the phase shifter, and finally the required data is measured. The novelty of the work is that the use of dark-bright soliton conversion to form the measurement system has never presented elsewhere. In this work, the simulation result is based on the use of practical device parameters, whereas the device fabrication to form the realistic device and application is plausible. The obtained output power of nW to μW is seen, which is available for single photon sensing application.

## 6.2 Sensors Using PANDA Ring Resonator

We have proposed the system of a nano-scale sensing transducer using PANDA ring resonator to make the benefit of the accuracy of measurements in nano-scale range, in which the sensing unit is consisted of an optical add/drop filter and two nanoring resonators, where one ring is placed as a transducer (sensing unit), the other ring is set as a reference ring. The system can provide the measuring regions with in the range of 1 nm, in which the self-calibration of the measurement of two sensing and reference signal can be compared without any additional optical part or other addition unit. The calibration is allowed by using the change in wavelength between sensing and reference signals, which is existed within the system.

## 6.3 Sensor via Wavelength Router

We propose a novel system of the dark soliton array generation using the multiplexed dark soliton pulses. The multi dark solitons are input into the series microring resonators where multiplexed and the filtering signals within add/drop ring system can be generated and obtained, which can be used to perform the large channel capacity in the secure communication link. In principle, dark soliton is one of the soliton properties where the soliton amplitude vanishes during the propagation in transmission line, which becomes an advantage over the bright soliton. Hence, the main difference between bright soliton and dark soliton properties is the dark soliton detection is extremely difficult, which is suitable for communication security applications. Thus, the channel spacing of the communication signals within a wavelength router can be provided by using the suitable free spectrum range. The other advantage is that the remote measurement and network sensor

are also available due to the use of the integrated optic device via multi wavelength router, which has shown the potential of broad applications in the near future.

## 6.4 Future Work

Optical tweezers are now widely used and they are particularly powerful in the field of microbiology to study cell–cell interactions, manipulate organelles without breaking the cell membrane and to measure adhesion forces between cells. In the next research we will describe a new concept of developing an optical tweezers source using a dark soliton pulse, which mean that the dynamic optical tweezers is plausible, therefore, the transportation of atoms/molecules in the optical network via a dark soliton being realized in the near future. In application, the trapped molecules/atoms by dynamic tweezers can be formed by using the tweezers array (multi tweezers), which is available for transportation in the routers [64] or optical wireless link [65]. The induced changes due to the surrounded environments can be measured and formed the molecules/atoms distributed sensors.

# REFERENCES


[1] Iizuka, T. and Kivshar, Yu. S. 1999. "Optical gap solitons in nonresonant quadratic media" **Phys. Rev.** E 59 : 7148–715.

[2] Ganapathy, R., Porsezian, K., Hasegawa, A., and Serkin, V. N. 2008. "Soliton interaction under soliton dispersion management" **IEEE J. Quantum Electron.** 44 : 383–390.

[3] Pornsuwancharoen, N., Dunmeekaew, U., and Yupapin, P.P. 2009. "Multi-soliton generation using a micro ring resonator system for DWDM based soliton communication" **Microw. & Opt. Tech. Lett.** 51(5) : 1374-1377.

[4] Yupapin, P.P., Pornsuwanchroen, N., and Chaiyasoonthorn, S. 2008. "Attosecond pulse generation using nonlinear micro ring resonators" **Microw. & Opt. Tech. Lett.** 50(12) : 3108-3011.

[5] Pornsuwancharoen, N. and Yupapin, P.P. 2009. "Generalized fast slow stop and store light optically within a nano ring resonator" **Microw. & Opt. Tech. Lett.** 51(4) : 899-902.

[6] Pornsuwancharoen, N., Chaiyasoonthorn S., and Yupapin, P.P. 2009. "Fast and slow lights generation using chaotic signals in the nonlinear micro ring resonators for communication security" **Opt. Eng.** 48(1) : 50005-1-5.

[7] Yupapin, P.P. and Pornsuwancharoen, N. 2009. "Proposed nonlinear micro ring resonator arrangement for stopping and storing light" **IEEE Photon. Tech. Lett.** 21 : 404-406.

[8] Sarapat, K., Sangwara, N., Srinuanjan, K., Yupapin, P.P. and Pornsuwancharoen, N. 2009 "Novel dark-bright optical soliton conversion system and power amplification" **Opt. Eng.** 48 : 045004.

[9] Yupapin, P.P. 2009 "Fiber optic sensing applications using the entangled state walk-off compensation" **Int. Light and Electron Opt.** 120 : 265-267.

[10] Yabosdee, P., Phophithirankarn, P. and Yupapin, P.P. 2010 "A new concept of nano-strain monitoring using μ strain perturbation" **Int. Light and Electron Opt.** 121 : 442-445

[11] Pornsuwancharoen, N., Phiphithirankarn, P., Yupapin, P.P. and Ali, J. 2009 "Pulse polarization entangled photon generated by chaotic signal in a nonlinear micro ring resonator for Birefringence based sensing applications" **Opt. and Laser Technol.** 41(6) : 788-793.

[12] Piyatamrong, B., Chat T., Jomtarak, R., Mitatha, S. and Yupapin, P.P. 2010 "Multi photons trapping within optical vortices in an add/drop multiplexer," **Opt. Lett.**, (in press)

[13] Phatharaworamet T., Chat T., Jomtarak, R., Mitatha, S. and Yupapin, P.P. 2010 "Random binary code generation using dark-bright soliton conversion control within a PANDA ring resonator" **IEEE J. Lightwave Technology**. (in press)

[14] Uomwech, K., Sarapat, K., and Yupapin, P.P. 2010 "Dynamic modutated Gaussian pulse propagation whith in the double PANDA ring resonator" **Microw. and Opt. Technol. Lett.** vol. 52 : 1818–1821.

[15] Udo, E. 1991. **Fibre optic sensors: an introduction for engineers and scientists.** Toronto:John Wiley & Sons.

[16] Krohn, D. A. 2000 **Fiber Optic Sensors: Fundamentals and Applications Instrumentation** Society of America Pbl., Research Triangle Park, NC.

[17] Yu, F. T. S., and Shizhuo, Y. 2002 **Fiber Optic Sensors** Marcel Decker, Inc., Newyork.

[18] Deng, D., and Guo, Q. 2007. "Ince-Gaussian solitons in strongly nonlocal nonlinear media" **Opt. Lett.** 32 : 3206-3208.

[19] Kokubun, Y., Hatakeyama, Ogata, Y., Suzuki, M., and Zaizen, N. 2005 "Fabrication technologies for vertically coupled micro ring resonator with multilevel crossing busline and ultracompact-ring radius" **IEEE J. Sel. Top. Quantum Electron.** 11 : 4–10.

[20] Su, Y., Liu, F., and Li, Q. 2007 "System performance of slow-light buffering, and storage in silicon nano-waveguide" **Proc. SPIE** 6783 : 67832P.

[21] Yupapin, P.P., Saeung, P., and Li, C. 2007 "Characteristics of complementary ring-resonator add/drop filters modeling by using graphical approach" **Opt. Commun.** 272 : 81-86.

[22] Yupapin, P.P. and Suwancharoen, W. 2007 "Chaotic signal generation and cancellation using a micro ring resonator incorporating an optical add/drop multiplexer" **Opt. Commun.**, 280(2) : 343-350.

[23] Agarwal, G. P. 2007 **Nonlinear Fiber Optics**, Academic Press, 4th ed., New York.

[24] Hasegawa A. 2000 **Massive, WDM and TDM Soliton Transmission Systems**, Kluwer Academic Publishers.

[25] Simonov, Yu. A. and Tjon, J. A. 1979 "Soliton-soliton interaction in confining models" **Phys. Lett.** B 85 : 380–384.

[26] Drohm, J. K., Kok, L. P., Simonov, Y. A., Tjon, J. A., and Veselov, A. I. 1981 "Collision, and rotation of solitons in three space-time dimensions" **Phys. Lett.** B 101 : 204–208.

[27] Rao, Y. J., Webb, D. J., Jackson, D. A., Zhang, L. and Bennion, I. 1998 "Optical in-fiber Bragg grating sensor systems for medical applications" **Biomedical Optics**, vol. 3 : 38-44.

[28] Grillet, A, Kinet, D., Witt, J., Schukar, M., Krebber, K., Pirotte, F. and Depre, A. 2008 "Optical fiber sensors embedded into medical textiles for healthcare monitoring," **IEEE J. Sensors**. vol. 8 : 1215-1222.

[29] Yi Cui, Qingqiao Wei, Hongkun Park, Charles M. Lieber, 2001 "Nanowire nanosensors for highly sensitive and selective detection of biological and chemical species," **Science**, vol. 293 : 1289-1292.

[30] Suchat, S., Khunnam, W. and Yupapin, P.P. 2009 "Self calibration in a fiber optic sensing system using the walk-off compensation" **Measurement**. vol. 42 : 1263-1267.

[31] Pornsuwancharoen, N. and Yupapin, P. P. 2009 "Generalized fast, slow, stop, and store light optically within a nanoring resonator" **Microw. and Opt. Technol. Lett.** vol. 51 : 899-902.

[32] Mitatha, S., Chaiyasoonthorn, N., and Yupapin, P. P. 2009 "Dark-bright optical solitons conversion via an optical add/drop filter" **Microw. and Opt. Technol. Lett.**, vol. 51 : 2104-2107.

[33] Agrawal G. P. 2007 **Nonlinear Fiber Optics**, 4th Edition, Academic Press.

[34] Hanim, S. F., Ali, J., and Yupapin, P. P. 2010 "Dark soliton generation using dual Brillouin fiber laser in a fiber optic ring resonator," **Microw. and Opt. Technol. Lett.**, vol. 52 : 881-883.

[35] Ali, J., and Yupapin, P. P. 2010 "An experimental investigation of multisoliton generation using an erbium-doped fiber amplifier and a fiber optic ring resonator," **Microw. and Opt. Technol. Lett.** vol. 52 : 70-72.

[36] Roy, S., Bhadra, S. K., and Agrawal, G. P. 2009 "Perturbation of higher-order solitons by fourth-order dispersion in optical fibers" **Opt. Commun.** vol. 282 : 3798–3803.

[37] Boucher, Y.G. and Feron, P. 2009 "Generalized transfer function: A simple model applied to active single-mode, microring resonators," **Opt. Commun**, vol. 282 : 3940–3947.

[38] Dumeige, Y., Arnaud, C., and Feron P. 2005 "Combining FDTD with coupled mode theories for bistability in micro-ring resonators," **Opt. Commun**, vol. 250 : 376–383.

[39] Maia T.T. et. al. 2010 "Optimization and comparison of photonic crystal resonators for silicon microcantilever sensors," **Sensors and Actuators A: Phys.** doi:10.1016/j.sna.2010.01.006

[40] Haque, M.A. and Saif, M.T.A. 2002 "Application of MEMS force sensors for in situ mechanical characterization of nano-scale thin films in SEM and TEM" **Sensors and Actuators A** vol. 97-98 : 239-245.

[41] Djinovic, Z., et. at. 2005 "Nanometer scale measurement of wear rate and vibrations by fiber-optic white light interferometry" **Sensors and Actuators A**, vol. 123–124 : 92–98.

[42] Yabosdee, P., Srinuanjan, K., and Yupapin, P.P. 2010 "Proposal of the nano-sensing device and system using a nano-waveguide transducer for distributed sensors," **Opt. Int. J. Light Electron.** doi:10.1016/j.ijleo.2009.07.013

[43] Berger, N. K. 2010 "Measurement of subpicosecond optical waveforms using a resonator-based phase modulator" **Opt. Commun** vol. 283 : 1397–1405.

[44] Ayca Yalcin 2006 "Optical sensing of biomolecules using microring resonators" **IEEE J. Selected topics in Quantum Electronics** 12 : 148-155

[45] Levinshtein, M., Rumyantsev, S., Shur, M. 1996 **Handbook Series on Semiconductor Parameters**, vol. 1, World Scientific, London, 147-168.

[46] Levinshtein, M., Rumyantsev, S., Shur, M. 1999 **Handbook Series on Semiconductor Parameters**, vol. 1, World Scientific, London, 153-179.

[47] Pearsall, T. P. 1982 **GaInAsP Alloy Semiconductors** John Wiley and Sons.

[48] Hua, P. at. al. 2002 "Integrated optical dual Mach–Zehnder interferometer sensor" **Sensors and Actuators B**, vol. 87 : 250–257.

[49] Ballav, M. and Chowdhury, A. R. 2006 "On a study of diffraction and dispersion managed soliton in a cylindrical media" **Progress In Electromagnetics Research, PIER** 63 : 33-50.

[50] Konar, S., and Biswas, A. 2005 "Soliton-soliton interaction with power law nonlinearity" **Progress In Electromagnetics Research, PIER** 54 : 95-108.

[51] Gangwar, R., Singh, S. P., and Singh, N. 2007 "Soliton based optical communication" **Progress In Electromagnetics Research, PIER** 74 : 157-166.

[52] Kivshar, Y. S., and Luther-Davies, B. 1998 "Dark optical solitons: Physics and applications" **Phys. Rep.** 298 : 81-197.

[53] Zhao, W. and Bourkoff, E. 1989 "Propagation properties of dark solitons" **Opt. Lett.**, Vol. 14 : 703-705.

[54] Barashenkov, I.V. 1996 "Stability criterion for dark soliton," **Phys. Rev. Lett.** 77 : 1193-1195.

[55] Christodoulides D.N. et. at. 1998 "Theory of incoherent dark solitons" **Phys. Rev. Lett.**, 80 : 5113-5115.

[56] Kim, A.D., Kath, W. L., and Goedde, C. G. 1996 "Stabilizing dark solitons by periodic phase-sensitive amplification" **Opt. Lett.**, 21 : 465-467.

[57] Malomed, B.A., Mostofi, A., and Chu, P. L. 2000 "Transformation of a dark soliton into a bright pulse" **J. Opt. Soc. Am. B** 17 : 507-513.

[58] Mithata, S., Pornsuwancharoen, N., and Yupapin, P. P. 2009 "A simultaneous short wave and millimeter wave generation using a soliton pulse within a nano-waveguide" **IEEE Photon. Technol. Lett.** 21(13) : 932-934.

[59] Mitatha, S. 2009 "Dark soliton behaviors within the nonlinear micro and nanoring resonators and applications" **Progress In Electromagnetic Research (PIER)** 99 : 383-404.

[60] Weiner A.M. et. at. 1988 "Experimental observation of the fundamental dark soliton in optical fibers" **Phys. Rev. Lett.** 61(21) : 2445-2448.

[61] Finot C. et. at. 2006 "Generation of dark solitons by interaction between similaritons in Raman fiber amplifiers" **Optical Fiber Technology** 12 : 217–226.

[62] Gharakhili, F.G., Shahabadi, M., and Hakkak, M. 2009 "Bright and dark soliton generation in a left-handed nonlinear transmission line with series nonlinear capacitors" **Progress In Electromagnetics Research, PIER** 96 : 237-249.

[63] Vongchumyen, C., Kulsirirat, K., Mitatha, S., and Yupapin, P.P. 2010 "Dark Soliton Multiplexing System for High Capacity and Security Communication within a Wavelength Router" **Optical Engineering** 49(05) : 055002.

# APPENDIX

## LIST OF PUBLICATIONS

1. Tamee, K.,Chaiyasoonthorn, S., Mitatha, S.,and Yupapin, P.P. 2010 "Nano-scale sensing transducer using entangled photon walk-off compensation" **International Journal of Light and Electron Optics** (Impact Factor:2008:0.507) (Article in press)
2. Tamee, K., Mitatha, S.,and Yupapin, P.P. 2010 "Distributed Photon Network Sensors via a Wavelength Router" **IET Wirel. Sens. Syst.** (Impact Factor:NA) (doi: 10.1049/iet-wss.2010.0046)
3. Tamee, K., Vongchumyen, C., Mitatha, S.,and Yupapin, P.P. 2011 "Sensors using Coincidence Dark-Bright Soliton Pair in a MZI" **International Conference on Embedded Systems and Intelligent Technology, ICESIT, Phuket, Thailand.** (Impact Factor:NA)
4. Tamee, K., Vongchumyen, C., Mitatha, S.,and Yupapin, P.P. 2011 "Molecular Distributed Sensors using Dark Soliton Array Trapping Tools" **International Conference on Embedded Systems and Intelligent Technology, ICESIT, Phuket, Thailand.** (Impact Factor:NA)
5. Tamee, K., Srinuanjan, K., Mitatha, S.,and Yupapin, P.P. 2010 "Distributed Sensors using a PANDA Ring Resonator Type in Multi Wavelength Router" **IEEE Sensors Journal** (Impact Factor:2009:1.610) (Article in press)

# BIOGRAPHY

**Date of Birth:** November 10th, 1975

**Born:** Bangkok Province, Thailand

**Current Address:** 27/17 Saimai75 Rd, Saimai, Bangkok, Thailand, 10220.

**E-mail:** kreangsakt@hotmail.com , kreangsakt@nu.ac.th

## Education

- Bachelors of Science (Physics), Faculty of Science, Chiang Mai University, Chiang Mai, Thailand, in 1998.
- Master of Engineering in Electrical Engineering, Faculty of Engineering, King Mongkut's Institute of Technology Ladkrabang, Bangkok, in 2001.

## Experience

- 8 year experience in the lecturer of Department of Computer Science and Information Technology, Faculty of Science, Naresuan University, Phitsanulok, Thailand

## Skilled Works

- Machine Learning
- Learning Classifier System
- Artificial Intelligence
- Neural Network & Fuzzy Set
- Nonlinear Optical, Optical Device Design & Simulation